NASA Contractor Report 145306

A PROCEDURE FOR THE DETERMINATION OF THE EFFECT OF FUSELAGE NOSE BLUNTNESS ON THE WAVE DRAG OF SUPERSONIC CRUISE AIRCRAFT

KENNETH B. WALKLEY

VOUGHT CORPORATION
Hampton Technical Center

3221 North Armistead Avenue • Hampton, Virginia 23666

an LTV Company

NASA CONTRACT NAS1-13500

JANUARY 1978

NASA
National Aeronautics and Space Administration

Langley Research Center
Hampton, Virginia 23665

FOREWORD

This document presents the results of a study to develop a procedure for the determination of the effect of fuselage nose bluntness on the wave drag of supersonic cruise aircraft. The Vought Corporation Hampton Technical Center provides technical support to the Advanced Supersonic Technology Office, Aeronautical Systems Division, NASA Langley Research Center under Contract Number NAS1-13500. The study was monitored by Mr. Vincent R. Mascitti of the Advanced Supersonic Technology Office. This report was prepared by Mr. Kenneth B. Walkley under the direction of Mr. C. W. Pearce, the Hampton Technical Center Advanced Aircraft Projects Supervisor.

TABLE OF CONTENTS

	Page
LIST OF FIGURES	iii
SUMMARY	1
INTRODUCTION	1
SYMBOLS	3
TECHNICAL APPROACH	4
Configuration Selection	4
Justification of Body-Alone Analysis	4
ANALYSIS AND RESULTS	5
Code Description and Capability	5
Demonstration of Code Applicability	6
Application to Present Study	7
Finite Difference Code Results	8
Sharp Nosed Fuselage	8
Blunt Nosed Fuselage	9
CONCLUDING REMARKS	10
REFERENCES	11
FIGURES	13
APPENDIX	A-1
Lighthill Equation and Numerical Approach	A-1
Accuracy and Convergence Characteristics	A-5
References	A-6
Figures	A-7
Computer Program	A-13

LIST OF FIGURES

Figure	Title	Page
1	The AST-100 Configuration	13
2	Near-Field Wave Drag for the AST-100.	14
3	Accuracy of the Finite Difference Codes as Applied to a Typical Blunted Cone	15
4	Afterbody Aerodynamics Using the Finite Difference Code	16
5	QUICK Code Modeling of the AST-100 Equivalent Fuselage.	17
6	Blunt Nose Geometry Definitions	18
7	Typical Blunt Nose Pressure Distributions Obtained from the Finite Difference Codes	19
8	Comparison of Computed Pressure Distributions for the Sharp Nosed Fuselage.	20
9	Wave Drag Variation with Mach Number for the Sharp Nosed Fuselage.	23
10	Computed Pressure Distributions for a Typical Blunted Fuselage.	24
11	Effect of Nose Bluntness on Fuselage Zero-Lift Wave Drag	27
12	AST-100 Configuration Drag Build-Up	28
A-1	Decay Function U(Z) for the Lighthill Integral.	A-7
A-2	Convergence Characteristics of the Lighthill Integral.	A-8
A-3	Pressure Coefficient Correlation for Minimum Drag Bodies	A-9
A-4	Wave Drag Correlation for Minimum Drag Bodies . .	A-10
A-5	Correlation of Afterbody Pressure Distributions .	A-11

A-6 Wave Drag Calculation for a Slender Area-Ruled Fuselage A-12

A PROCEDURE FOR THE DETERMINATION OF THE EFFECT OF FUSELAGE NOSE BLUNTNESS ON THE WAVE DRAG OF SUPERSONIC CRUISE AIRCRAFT

By Kenneth B. Walkley

Vought Corporation Hampton Technical Center

SUMMARY

The incremental wave drag penalty due to nose blunting of a fuselage has been investigated using a three-dimensional finite difference scheme. An aircraft typical of current supersonic cruise concepts has been considered. Computational problems with the finite difference scheme as the fuselage afterbody closes have been addressed. A linear theory method has been employed to compute the afterbody aerodynamics and effectively extends the finite difference scheme to closing afterbodies. Acceptable drag increments for various levels of nose bluntness have been demonstrated using this approach.

INTRODUCTION

The ability to predict the effect of nose bluntness on the wave drag of supersonic cruise aircraft is important for the aircraft designer. Recent studies of sonic boom minimization (references 1 and 2) stress the importance of nose bluntness in reducing overpressure levels. Continuing NASA low speed aerodynamics tests (reference 3) are aimed at achieving low attitudes in the approach and landing condition for supersonic cruise aircraft. These low attitudes coupled with nose blunting could simplify a complex mechanical visor nose which is now required for aircraft such as the Anglo-French Concorde. Reduced attitudes which maintain good pilot visibility could result in reduced weight and complexity, shorter landing gear struts, and improved performance. These potential benefits for supersonic cruise aircraft will be paced, however, by the increases in wave drag associated with blunting of the nose.

Many methods for the calculation of blunt nose aerodynamics for bodies of revolution exist in the literature (see references 4, 5, 6, 7, and 8 for example). Although the accuracy of these various methods has been substantiated, application to specific aircraft designs at arbitrary supersonic Mach numbers in a straightforward manner is not usually possible. The finite difference relaxation method of reference 4, for example, applies to transonic Mach numbers only while for flight conditions below Mach 3.0, the method of characteristics approach of reference 5 is not generally applicable. Similarly, only the blunt nose of a fuselage may be analyzed using the procedures described in references 6 and 7. The method of reference 8 allows for an arbitrary afterbody shape, but no results for fuselage type bodies with closure are presented. All of these methods are available in computer program form, but both specific input requirements as well as the associated program output data vary considerably. Often program output is not in a form which is conveniently usable by the aircraft designer.

The three-dimensional finite difference codes of reference 9 overcome some of the shortcomings noted above and provide the means for a relatively straightforward analysis of complex aircraft geometries including the effects of nose bluntness. The purpose of this paper is to present the results of an analysis of nose bluntness effects for a supersonic cruise vehicle using the finite difference codes of reference 9. An assessment of the accuracy of the codes is also considered through comparisons with both experimental data and a linear theory method.

The author wishes to acknowledge the contributions to this document of Vincent R. Mascitti of the NASA Langley Research Center. Mr. Mascitti developed the numerical approach for applying the Lighthill integral to arbitrary axisymmetric bodies. The Appendix of this paper summarizes the development of this method. His suggestions and guidance during the course of this effort are greatly appreciated.

SYMBOLS

C_D	drag coefficient
C_{D_i}	drag due to lift
$C_{D_{interference}}$	interference drag coefficient
$C_{D_{friction}}$	skin friction drag coefficient
$C_{D_{wave}}$	wave drag coefficient
$\Delta C_{D_{nose\ bluntness}}$	incremental wave drag coefficient due to nose bluntness
C_L	lift coefficient
$C_{p_{surface}}$	body pressure coefficient
d_{max}	body maximum diameter
ℓ	body length
M_∞	freestream Mach number
R_{base}	body base radius
R_{max}	body maximum radius
R_{nose}	blunt nose radius
s	distance along body meridian measured from the nose
S_{ref}	reference area
x	longitudinal coordinate
α	body angle of attack

TECHNICAL APPROACH

Configuration Selection

A configuration typical of current AST (Advanced Supersonic Technology) design concepts has been chosen as the basis for this analysis. Both the original sharp nosed fuselage and four blunt nosed variations have been studied at Mach numbers of 2.7, 2.2, and 1.7 to assess the incremental wave drag penalties associated with nose bluntness. All drag coefficients presented herein are based on the configuration wing reference area and may be applied directly to the complete configuration.

The AST-100 is a 292-passenger concept designed for Mach 2.7 cruise at 18,288 m (60,000 ft). A complete description and analysis of this configuration has been presented in reference 10, and a three-view drawing of the aircraft is presented in Figure 1. Of particular interest to this study is the fuselage. This high fineness ratio body (ℓ/d_{max} = 25.5) is circular in cross-section except in the mid-region where it is slightly elliptical. The fuselage is also cambered for integration with the theoretical wing root camber and area-ruled for minimum overall configuration wave drag at the Mach 2.7 cruise condition. The baseline fuselage employs a sharp nose-aligned with the freestream flow. For analysis purposes, this fuselage has been modeled as an uncambered body of revolution with the appropriate area distribution. An angle of attack of zero degrees has been assumed throughout the analysis.

Justification of Body-Alone Analysis

The purpose of the analysis has been to evaluate the incremental drag penalties associated with various levels of nose bluntness relative to the baseline sharp nose. These penalties have been assessed through analysis of the wave drag characteristics of the fuselage alone. The validity of this approach has been demonstrated experimentally for a wing-body in reference 11. At Mach 1.61 these results indicated that nose blunting had no interference effects on the wing at zero angle of attack. This conclusion is further substantiated in Figure 2 for the AST-100 where both configuration wave drag and interference drag data are presented for a range of supersonic Mach

numbers. These results have been obtained using the near-field wave drag analysis method presented in reference 12. This method assumes zero-lift conditions and calculates the thickness and interference pressure distributions for the configuration with zero wing and fuselage camber. The resultant drag force is obtained by integrating the pressure distributions over the components cross-sectional areas. Figure 2 shows that for the complete configuration the interference drag coefficients are bounded in magnitude by two drag counts (±.0002) whereas for the wing-body alone, the total interference drag coefficient is less than one drag count (.0001) for the Mach number range of interest. These results indicate that much of the interference drag occurs between the nacelles and other aircraft components. It is assumed that these nacelle terms are not appreciably influenced by changes in the local flow at the nose, and thus a reasonable approach to the current problem is to consider the fuselage alone. Variations in the fuselage drag levels due to nose bluntness thus can be applied directly to the baseline configuration drag levels.

ANALYSIS AND RESULTS

Consideration of the present need to analyze flows over blunt nosed bodies of revolution for which the linear theory is inapplicable has resulted in the choice of a three-dimensional finite difference scheme for calculation of the fuselage aerodynamics. The method chosen has been documented in reference 9 while an abbreviated description of the method and correlations of the theoretical results with experimental data have been presented in reference 13. A recent review of efforts with these finite difference codes as applied to supersonic cruise aircraft has been published as reference 14.

Code Description and Capability

The finite difference code is comprised of five separate computer programs, three of which have been employed herein. The QUICK code provides the means for modeling relatively complex geometries and providing the continuous analytic definition required by the other codes. Computation of the super/hypersonic flows about rather arbitrary configurations over a wide range of

Mach numbers and angles of attack is handled by the STEIN code. Use of this program first requires a complete definition of the flow field at a starting plane location near the nose of the configuration. A routine for definition of this starting plane for sharp circular cones at small angles of attack is provided within the STEIN code itself. Starting plane data for flows over blunt noses is generated using the BLUNT code which is compatible with both the QUICK and STEIN programs (the BLUNT code is based on reference 7). Once the starting plane data is defined, the STEIN code computes the complete flow field between the configuration and the associated shock envelope from the starting plane to a specified end station. Additional details on the theory and computational techniques employed in these methods may be obtained from the references cited above.

Demonstration of Code Applicability

Blunt cone pressure distributions have been computed at Mach numbers of 2.96, 2.30, and 1.90 using the BLUNT and STEIN codes to demonstrate their applicability to the present effort. The geometry of the blunted cone considered and the results obtained are presented in Figure 3. The experimental data have been obtained from reference 8. The agreement between the theoretical estimates and the measured data is quite good at all Mach numbers considered. Difficulty with execution of the BLUNT code occurs as the Mach number is decreased below 1.90, and no solution was obtained at Mach 1.50. Current efforts toward extending the applicability of the BLUNT code to these lower supersonic Mach numbers are continuing at the NASA Langley Research Center, but no attempt to obtain solutions for the present problem using the revised methods have been made.

The capability of the finite difference code to predict afterbody aerodynamics is demonstrated in Figure 4. The experimental data shown have been obtained by William K. Abeyounis of the NASA Langley Research Center and are unpublished. The agreement between the theory and experiment is excellent to within approximately ten percent of the body closure point. The computed pressure coefficients then increase rapdily, and the program actually terminates due to numerical errors prior to computation at the closure point.

Afterbody closure effects in supersonic flows have been investigated by Meyer (reference 15) and Reyn (reference 16). Both authors point to the possibility of the formation of a region of subsonic flow ahead of the body closure point. The region is preceded by an attached tail shock and is followed by a sonic line. If such a subsonic region does occur on the fuselage under consideration, the STEIN code cannot continue to compute. Existence of this subsonic region thus provides a plausible explanation for the failure of the STEIN code near the rear closure point. A procedure for effectively extending the finite difference scheme to closing afterbodies is presented below in the application of the theory to the AST-100 fuselage.

Application to Present Study

The uncambered, circular cross-section representation of the AST-100 fuselage has been modeled in two parts using the QUICK code as shown in Figure 5. A two-part definition is required to attain the desired level of accuracy in the model while not exceeding the QUICK code limitations on the maximum number of arcs allowed for the geometry definition. As Figure 5 shows, good accuracy in the model radius distribution has been achieved using a combination of linear segments connected by second-order fairings. This sharp nosed fuselage has been blunted as shown in Figure 6. The associated reduction in fuselage length and fineness ratio are also summarized in Figure 6. The body definition aft of the various blunt noses remains unchanged relative to the original sharp nose in all cases.

Required starting plane solutions have been computed using the STEIN and BLUNT codes as previously described. The choice of the starting plane location is arbitrary although some care must be exercised with the blunt noses to insure that the axial component of the Mach number at the starting plane is supersonic. Pressure distributions typical of those obtained are shown in Figure 7. Experience with the BLUNT code has indicated that the axial Mach number at the starting plane must be "sufficiently" supersonic to achieve successful execution of the STEIN code on subsequent runs. In particular, it may be necessary to move the starting plane location further downstream for the blunt noses as the freestream Mach number is decreased in

order to obtain a reasonable starting plane Mach number.

Having defined the necessary starting plane data for the various geometries, the STEIN code has been used to compute the body pressure distributions and associated wave drag coefficients. It should be noted that two executions of the STEIN code are required for computation of the flow field over the entire body length because of the two-segment geometry definition. This procedure is relatively straightforward in that the flow field at any intermediate body station may be saved on punched cards, magnetic tape, or disk, and then used to restart the code for subsequent calculations. This approach does increase analysis time, however, due to the relatively long turnaround times currently associated with the STEIN code.

Finite Difference Code Results

Sharp Nosed Fuselage - Computed surface pressure distributions at Mach numbers of 2.7, 2.2, and 1.7 are presented in Figure 8. Results obtained from both the STEIN code and the linear theory Lighthill integral method are shown. A detailed description of the Lighthill method as well as demonstrations of its applicability and accuracy are included in the Appendix. The STEIN code results have been obtained using 900 mesh points over the forward portion of the fuselage and 1800 over the aft section. This increase in the number of mesh points is required because of the relatively large distances between the body and shock toward the fuselage aft section. The Lighthill solution has been obtained using 501 points to represent the body. The QUICK geometry modeling has been employed for both methods. As Figure 8 shows, the pressure distributions computed with these two methods agree quite well over the majority of the body length. Both methods encounter some difficulty as the rear stagnation point is appraoched, however. The STEIN code result appears to be more sensitive to the body closure, and the computed pressure coefficient instability becomes more acute as the Mach number decreases. As previously noted, the STEIN code is unable to compute the flow field to the end of the body, and the program stops with a numerical error exit prior to the closure point. The Lighthill method does compute the pressure distribution to a point arbitrarily close to the body closure point, but the magnitudes of the

computed values can become relatively large.

As shown in Figure 9, both the magnitude and trend of the wave drag coefficients computed by the STEIN code disagree markedly with results obtained using the Lighthill method. This result is to be expected, however, as the code failure at the rear of the fuselage results in large positive pressures which provide an erroneous thrust. If these aft pressures (for fuselage stations beyond 73 m (240 ft) for example) are replaced with the values computed using the Lighthill theory, results which closely agree with the Lighthill values can be obtained as shown in Figure 9.

Blunt Nosed Fuselage - Figure 10 presents typical comparisons of the pressure distributions computed using the BLUNT and STEIN codes for the blunt nosed fuselage R_{nose}/R_{max} = .246 and the original sharp nosed case. Note that the origin of the sharp nosed body has been shifted to the left to maintain geometric correspondence between the two bodies. Comparison of these pressure distributions shows that the blunt nosed fuselage pressure distributions correspond to the sharp nosed solution at the same Mach number for points downstream of the nose region, and that the effects of nose blunting tend to be localized on the forebody. This result further confirms the previous conclusion that changes to the nose geometry do not result in appreciable interference on the wing.

The total drag for the blunt nosed fuselages has been computed using the BLUNT and STEIN codes pressures aft to approximately station 73 m (240 ft) and then substituting the Lighthill values as was done for the sharp nosed cases. The results of this analysis are summarized in Figure 11 where the incremental wave drag coefficient due to blunting is presented. There appears to be a negligible drag penalty for noses with bluntness values less than about 0.15, but the incremental drag then increases at a fairly high rate.

The relative magnitudes of these drag increments are illustrated in Figure 12 where typical values of skin friction, wave drag, and drag-due-to-lift are presented for the AST-100 configuration. Reasonable nose bluntness levels would results in additional drag penalties of less than ten percent of the configuration total drag at the Mach 2.7 cruise condition.

CONCLUDING REMARKS

The incremental wave drag penalty due to nose blunting of a fuselage has been investigated using a three-dimensional finite difference scheme. An aircraft typical of current supersonic cruise concepts has been considered. The analysis assumes that the incremental drag value may be determined by considering the fuselage alone.

The finite difference scheme provides an exact inviscid solution for the blunt nose and forebody, but computational problems occur near the afterbody closure point. The existence of a region of subsonic flow has been postulated as a possible cause of the failure of the finite difference scheme in this area. A linear theory method has been used to compute the afterbody aerodynamics for the sharp nosed fuselage. These results may then be matched with the finite difference scheme ahead of the afterbody to obtain the complete fuselage pressure distribution and wave drag. This approach is also valid for the blunt nosed fuselages since the effects of blunting are shown to be localized on the forebody.

Acceptable drag increments for various levels of nose bluntness have been demonstrated for a typical supersonic cruise concept using these modified finite difference code pressure distributions. The relative importance of these drag increments will generally depend on the specific vehicle application, however.

A possible extension of the present method would utilize the finite difference codes to compute the aerodynamics for the blunt nose with the linear theory method providing pressures for the remainder of the body. This approach would probably be the most convenient and computationally efficient.

REFERENCES

1. Seebass, R. and George, A. R.: Sonic Boom Minization. J. Acoust. Soc. Amer. Volume 51, No. 2, Pt. 3, February 1972, pp. 686-694.

2. Darden, Christine M. and Mack, Robert J.: Current Research in Sonic Boom Minimization. Proceedings of the SCAR Conference, NASA CP-001, 1976.

3. Coe, Paul L., Jr. and Graham, A. B.: Results of Recent NASA Research on Low-Speed Aerodynamic Characteristics of Supersonic Cruise Aircraft. Proceedings of the SCAR Conference, NASA CP-001, 1976.

4. South, Jerry C., Jr. and Jameson, Antony: Relaxation Solutions for Inviscid Axisymmetric Transonic Flow over Blunt or Pointed Bodies. Proceedings of the AIAA Computational Fluid Dynamics Conference, 1973.

5. Inouye, Mamoru; Rakich, John V.; and Lomax, Harvard: A Description of Numerical Methods and Computer Programs for Two-Dimensional and Axisymmetric Supersonic Flow over Blunt-Nosed and Flared Bodies. NASA TN D-2970, 1965.

6. Zoby, Ernest V. and Graves, Randolf, A., Jr.: A Computer Program for Calculating the Perfect Gas Inviscid Flow Field About Blunt Axisymmetric Bodies at an Angle of Attack of 0°. NASA TM X-2843, 1973.

7. Moretti, Gino and Bleich, Gary: Three-Dimensional Flow Around Blunt Bodies. AIAA Journal, Volume 5, No. 9, September 1967.

8. Jackson, Charlie M., Jr.; Sawyer, Wallace C.; and Smith, Rudeen S.: A Method for Determining Surface Pressures on Blunt Bodies of Revolution at Small Angles of Attack in Supersonic Flow. NASA TN D-4865, 1968.

9. Marconi, Frank; Salas, Manuel; and Yaeger, Larry: Development of a Computer Code for Calculating the Steady Super/Hypersonic Inviscid Flow Around Real Configurations. Two Volumes, NASA CR-2675 and 2676, 1976.

10. Baber, H. T., Jr. and Swanson, E. E.: Advanced Supersonic Technology Concept AST-100 Characteristics Developed in a Baseline-Update Study. NASA TM X-72815, January 16, 1976.

11. Gapcynski, John P. and Robins, A. Warner: The Effect of Nose Radius and Shape on the Aerodynamic Characteristics of a Fuselage and a Wing-Fuselage Combination at Angles of Attack. NACA RM L53I23a, 1953.

12. Middleton, W. D.; Lundry, J. L.; and Coleman, R. G.: A Computational System for Aerodynamic Design and Analysis of Supersonic Aircraft. Three Parts - NASA CR-2715, -2716, and -2717, July 1976.

13. Marconi, F.; Yaeger, L.; and Hamilton, H. H.: Computation of High-Speed Inviscid Flows about Real Configurations. Proceedings of the Conference on Aerodynamic Analyses Requiring Advanced Computers, Part II, NASA SP-346, 1975, pp. 1411-1455.

14. Townsend, J. C.: The Role of Finite Difference Methods in Design and Analysis for Supersonic Cruise. Proceedings of the SCAR Conference, NASA CP-001, 1976.

15. Meyer, R. E.: Tail Shock Problem, Physics of Fluids, Volume 7, No. 8, p. 1219, August 1964.

16. Reyn, J. W.: Compressible Inviscid Flow Near the End of Pointed After-bodies. J. Aero. Sci., Volume 25, No. 12, p. 787, December 1958.

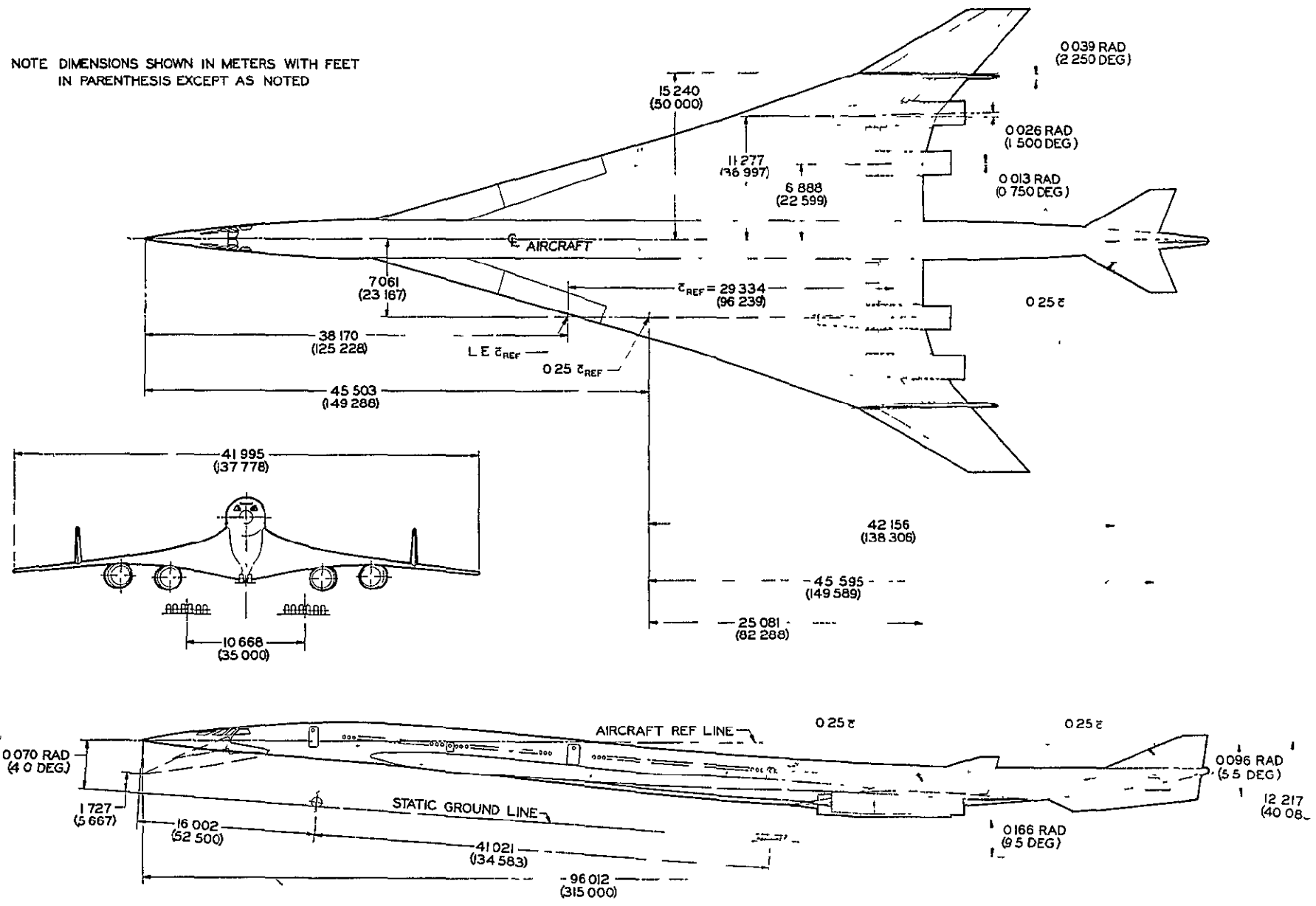

Figure 1. The AST-100 Configuration

AST-100

S_{REF} = 926.15 m^2 (9969 ft^2)

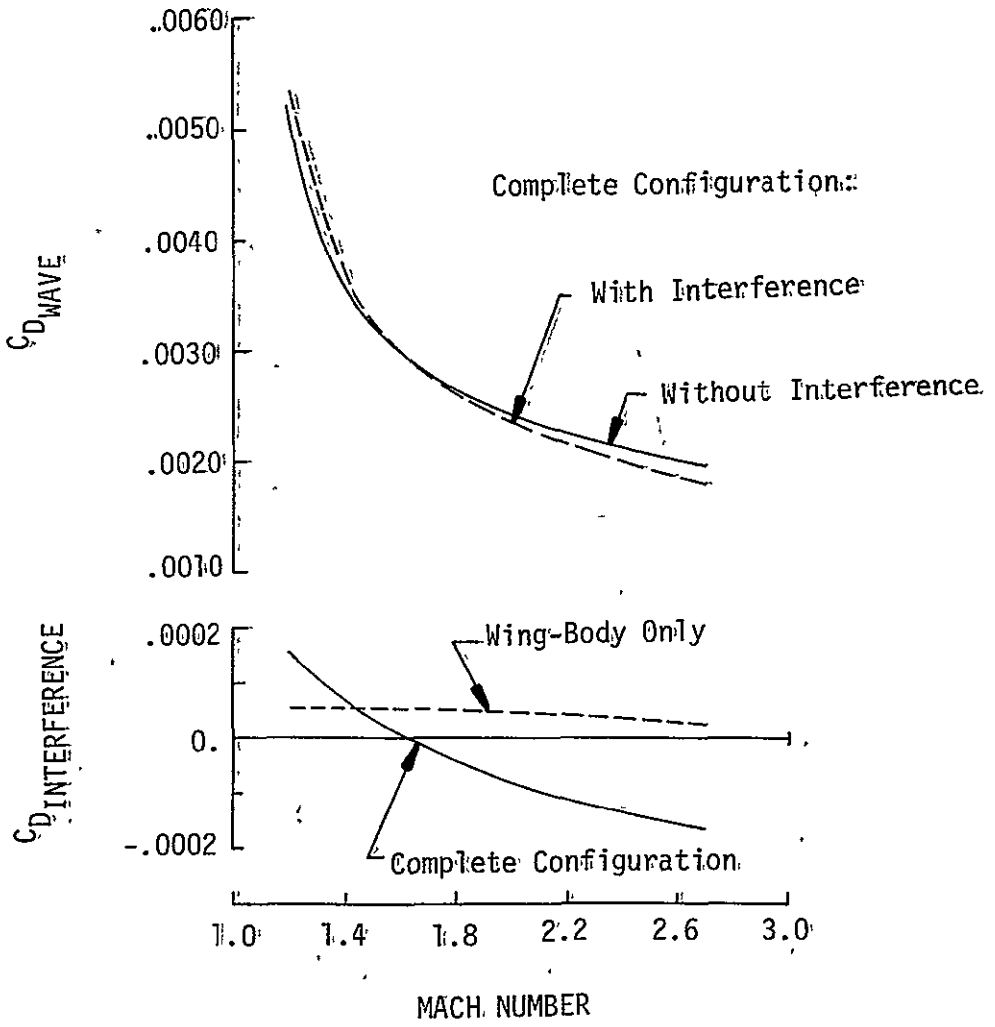

Figure 2. Near-Field Wave Drag for the AST-100

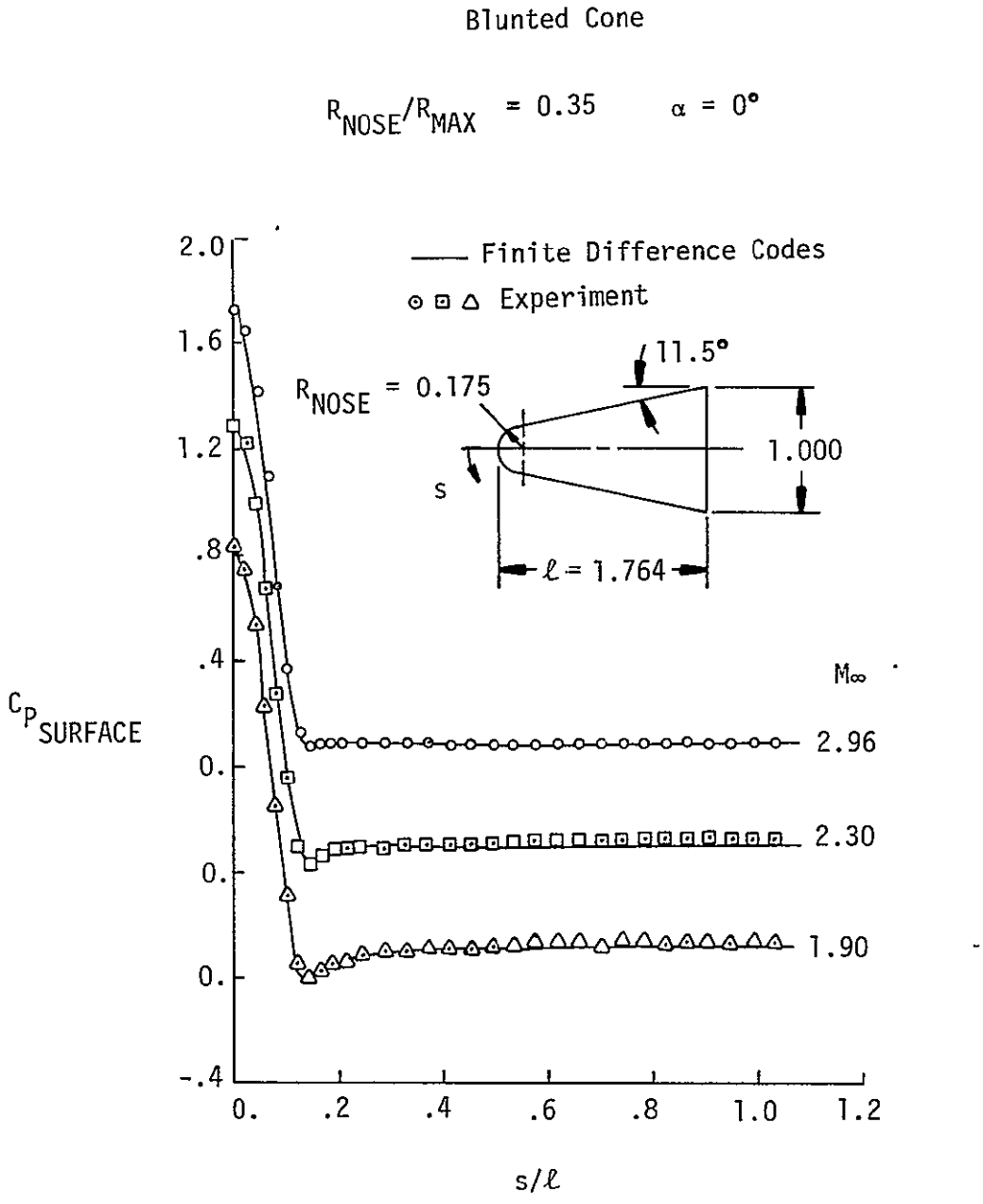

Figure 3. Accuracy of the Finite Difference Codes as Applied to a Typical Blunted Cone

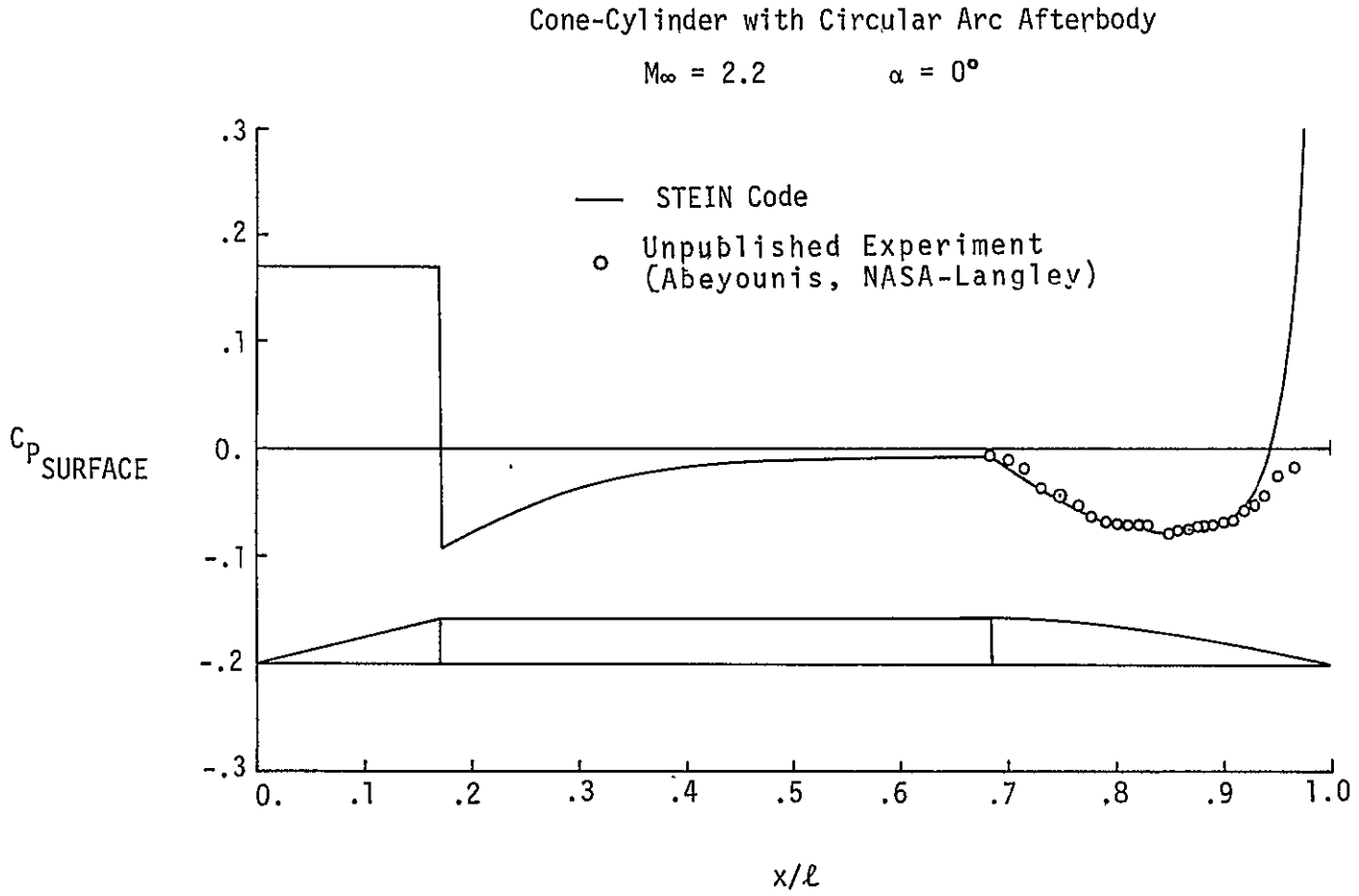

Figure 4. Afterbody Aerodynamics Using the Finite Difference Code

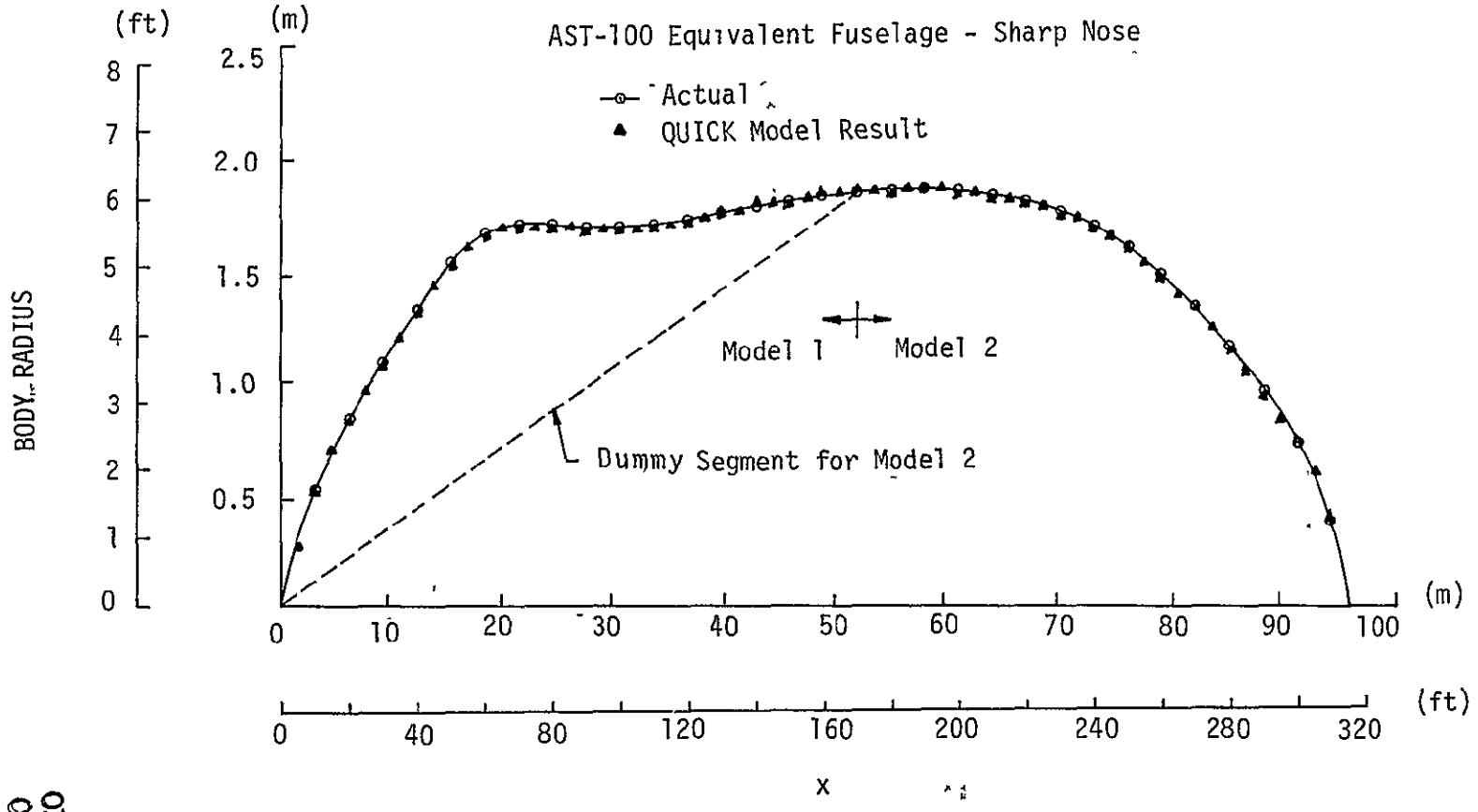

Figure 5. Quick Code Modeling of the AST-100 Equivalent Fuselage

AST-100 Equivalent Fuselage

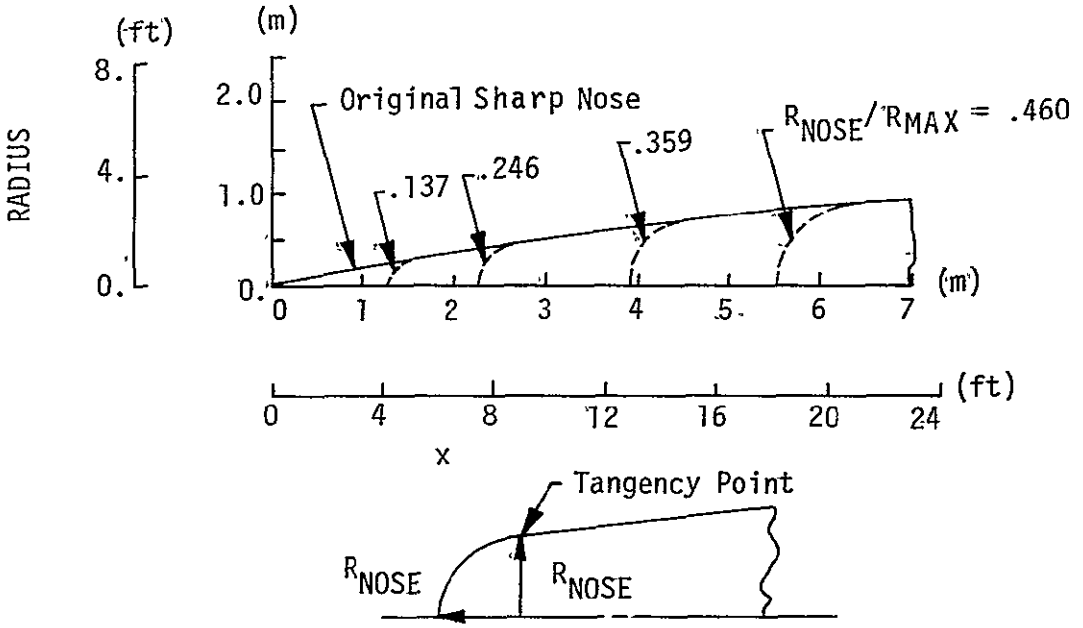

Fuselage Maximum Radius ~ R_{MAX} = 1.884 m (6.180 ft)

$\frac{R_{NOSE}}{R_{MAX}}$	Fuselage Length m (ft)	Fineness Ratio
Sharp	96.0 (315.0)	25.5
.137	94.7 (310.8)	25.1
.246	93.7 (307.5)	24.9
.359	92.1 (302.3)	24.5
.460	90.5 (296.8)	24.0

Figure 6. Blunt Nose Geometry Definitions

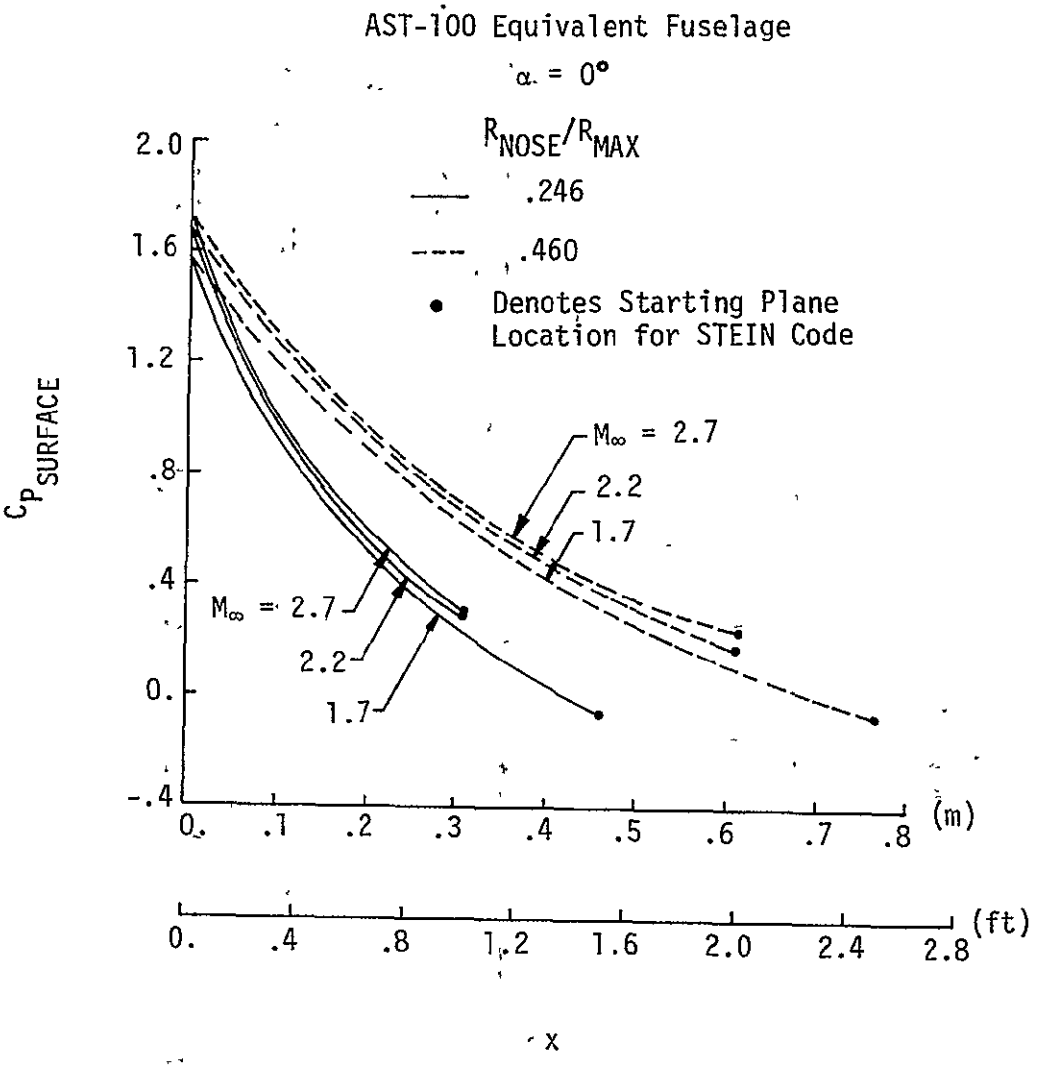

Figure 7. Typical Blunt Nose Pressure Distributions Obtained from the Finite Difference Code

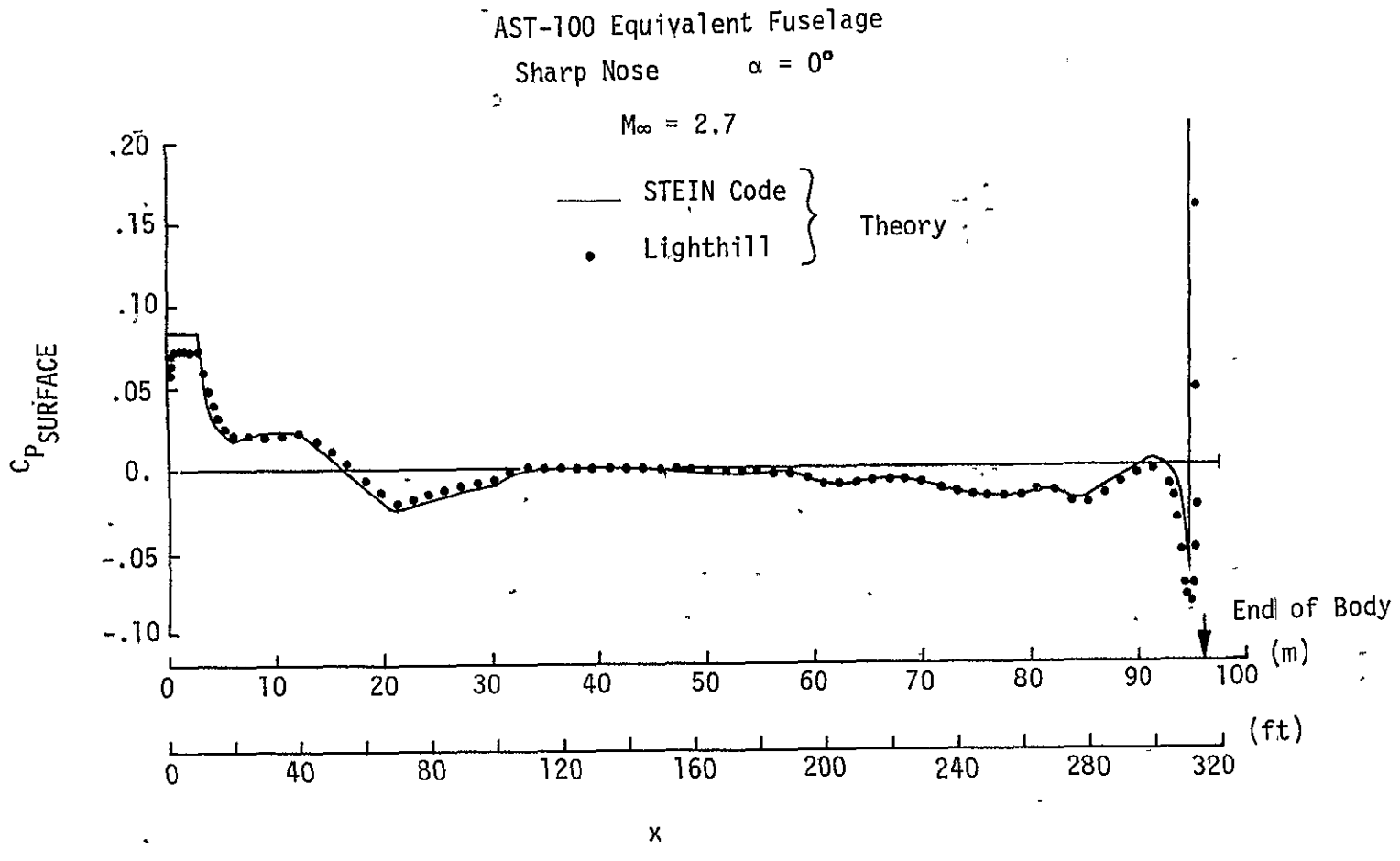

Figure 8. Comparison of Computed Pressure Distributions for the Sharp Nosed Fuselage

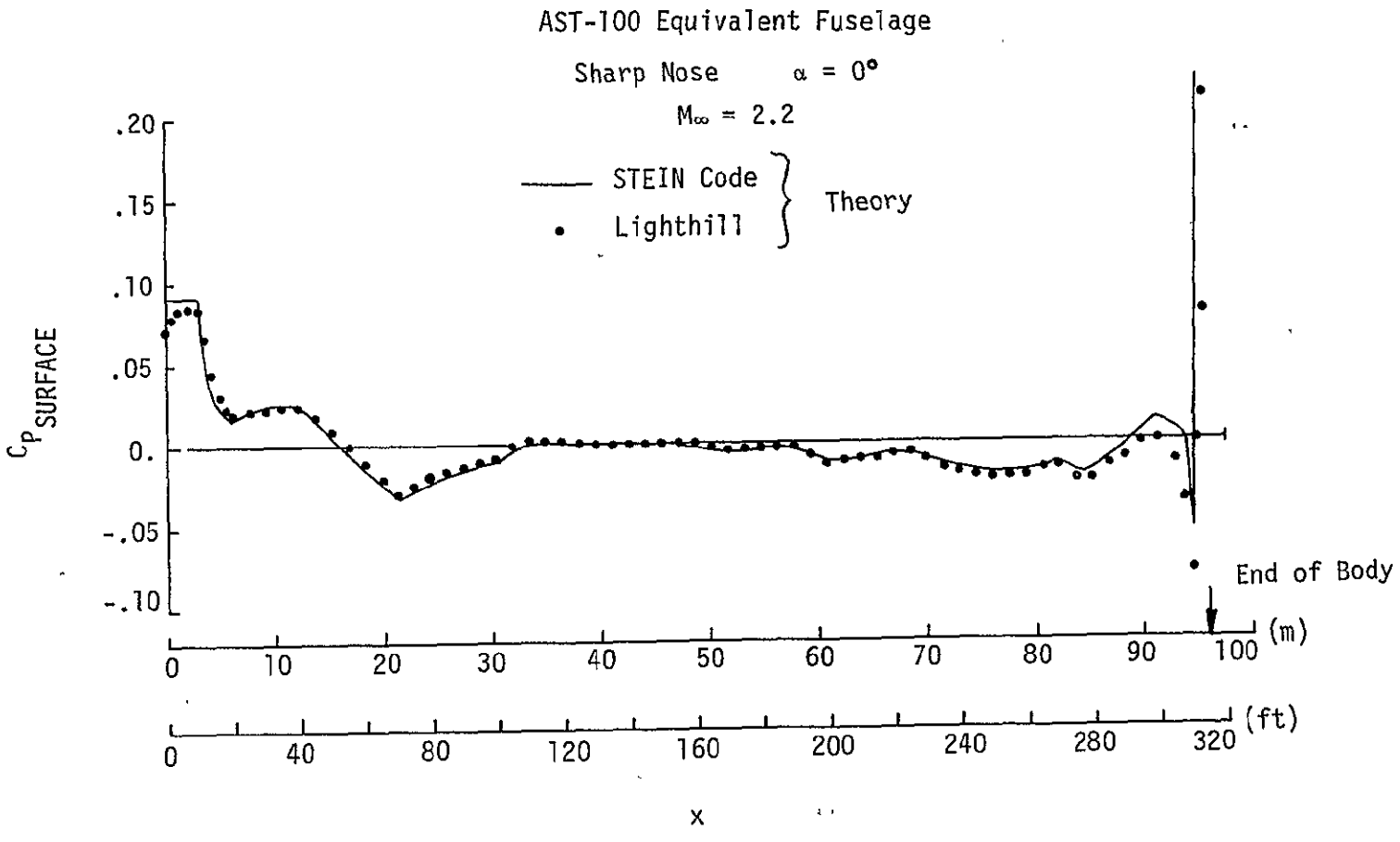

Figure 8. Continued

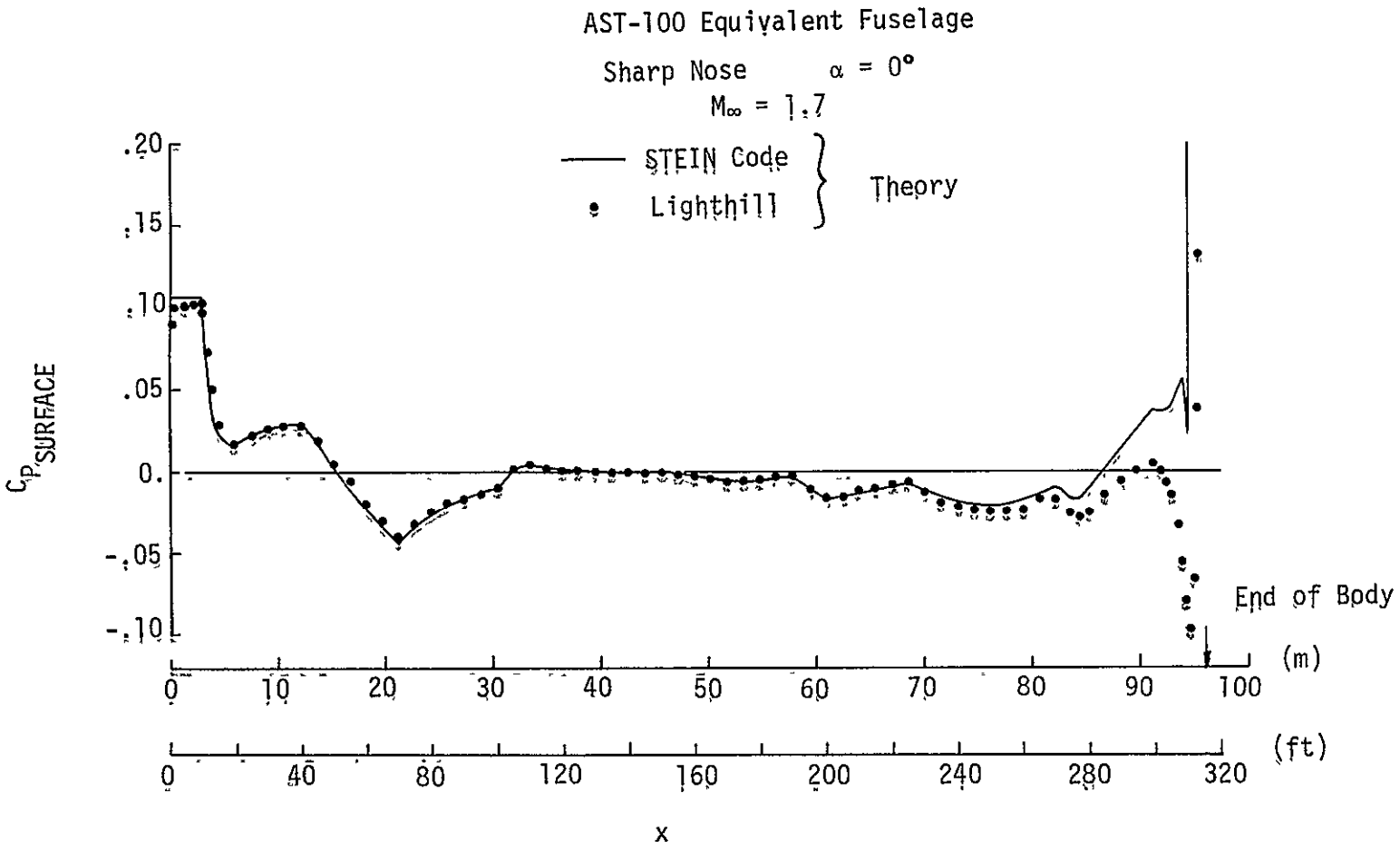

Figure 8. Concluded

AST-100 Equivalent Fuselage

S_{REF} = 926.15 m^2 (9969 ft^2)

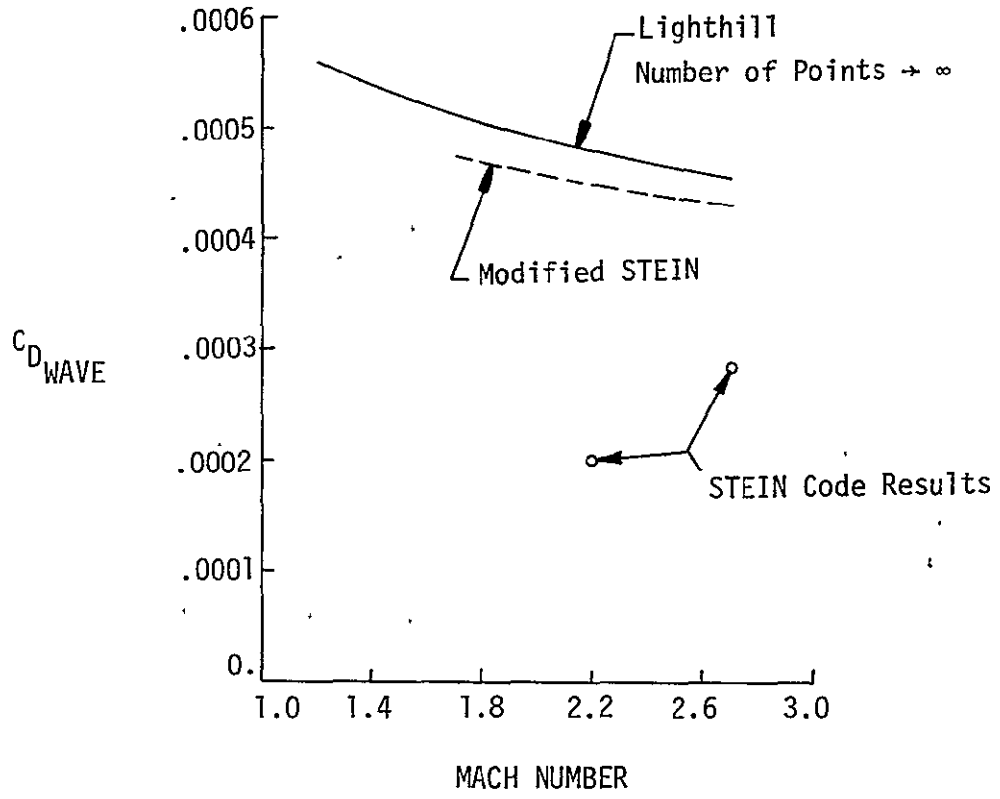

Figure 9. Wave Drag Variation with Mach Number for the Sharp Nosed Fuselage

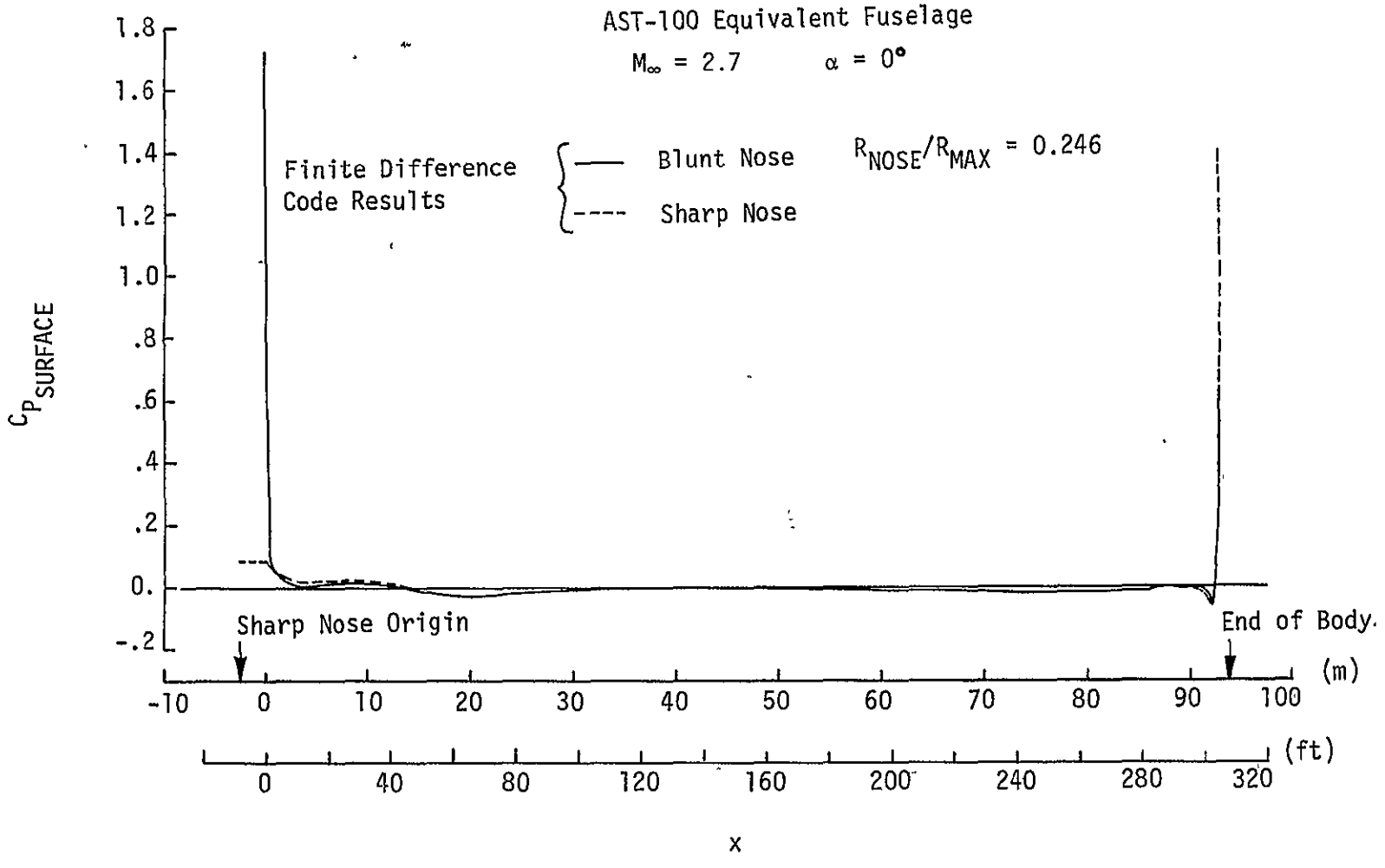

Figure 10. Computed Pressure Distribution for a Typical Blunted Nose

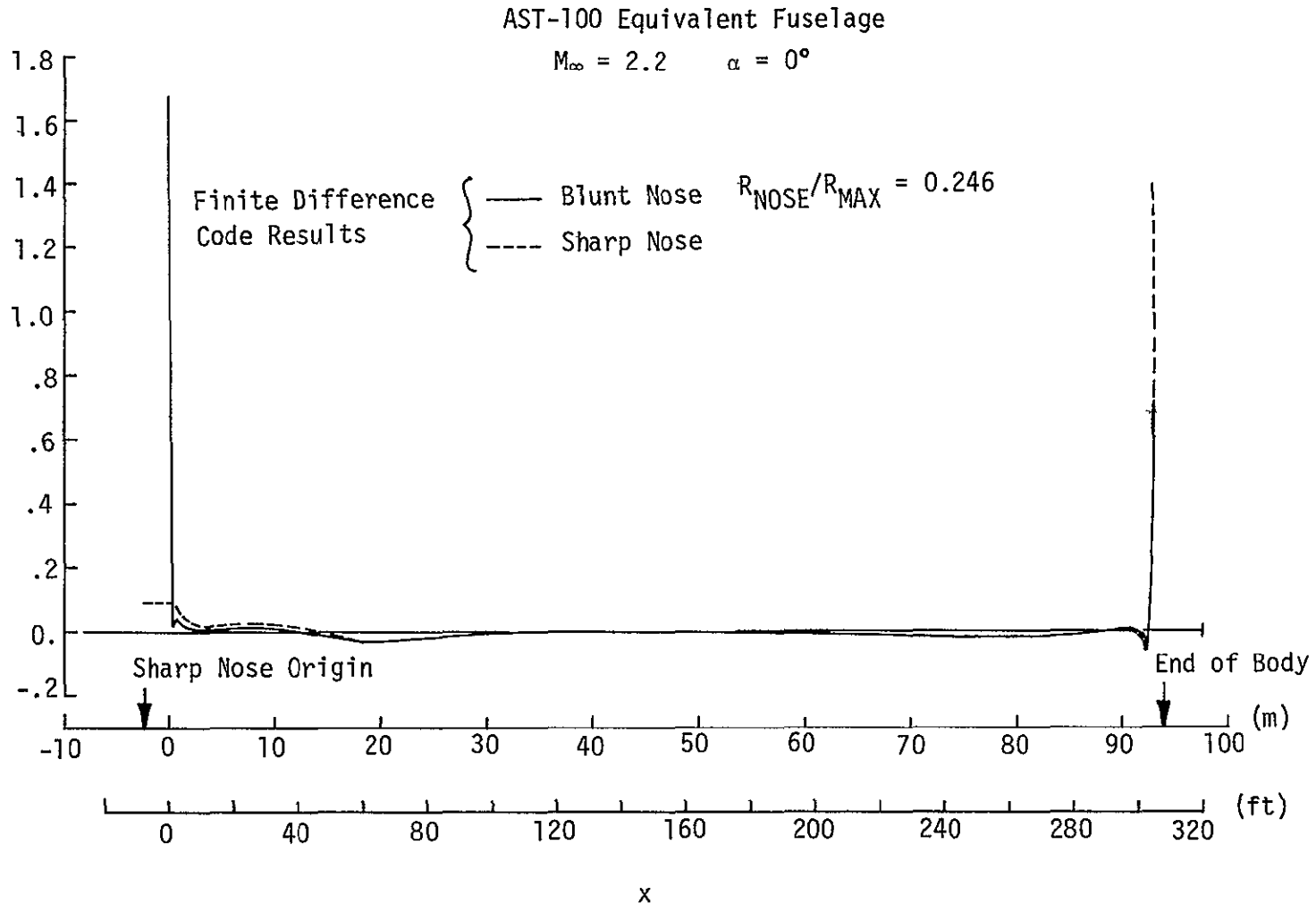

Figure 10. Continued

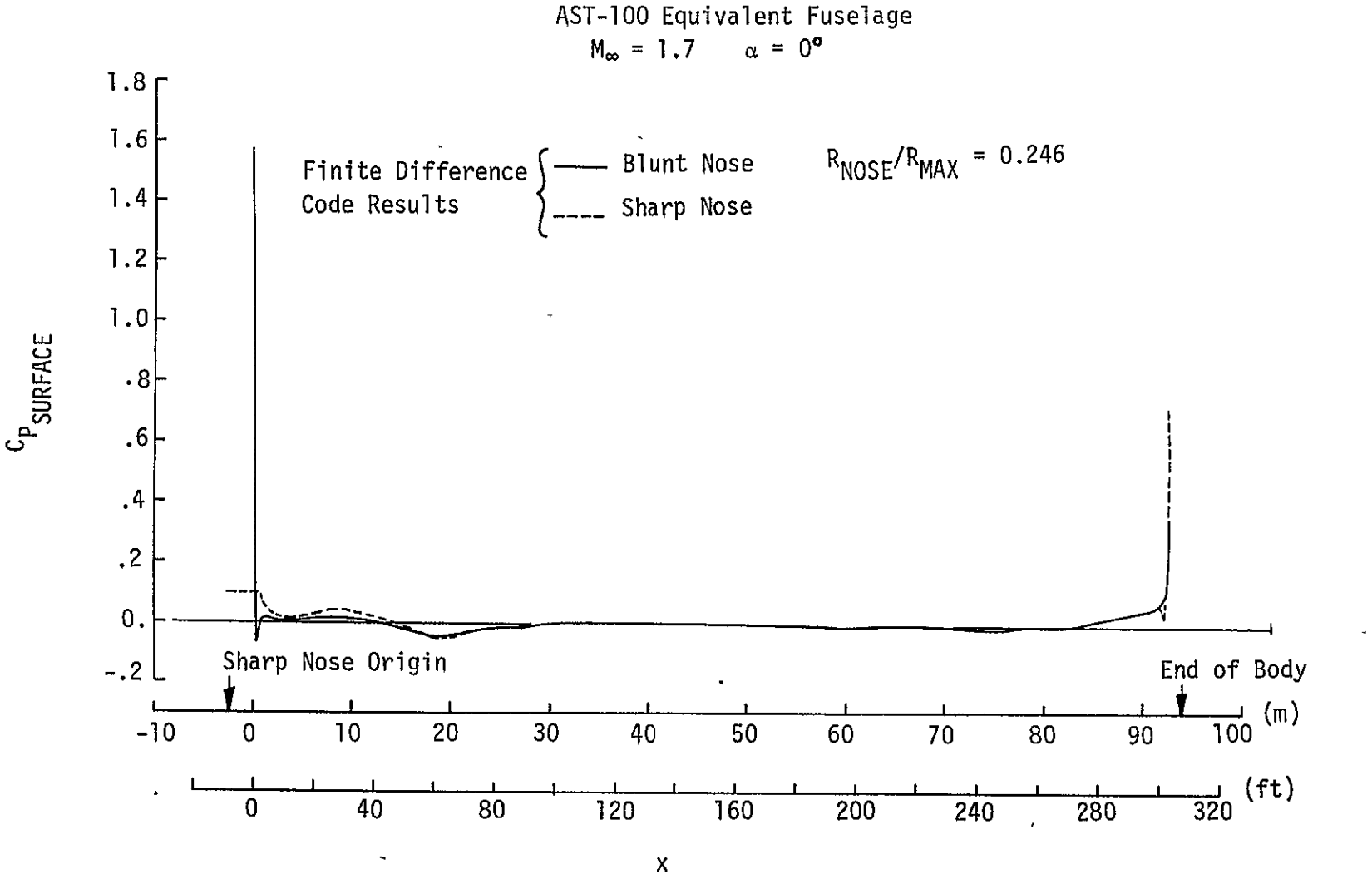

Figure 10. Concluded

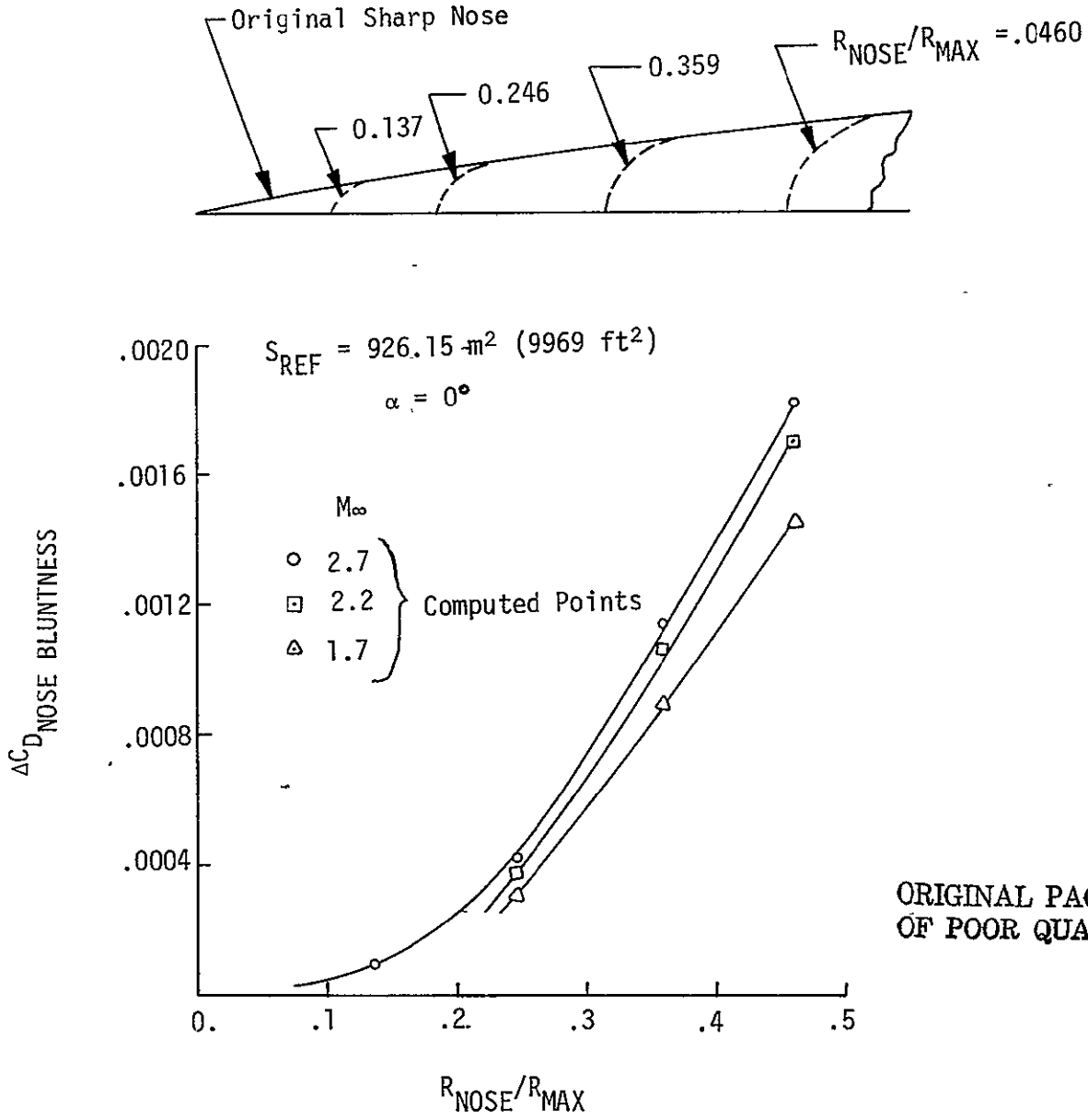

Figure 11. Effect of Nose Bluntness on Fuselage Zero-Lift Wave Drag

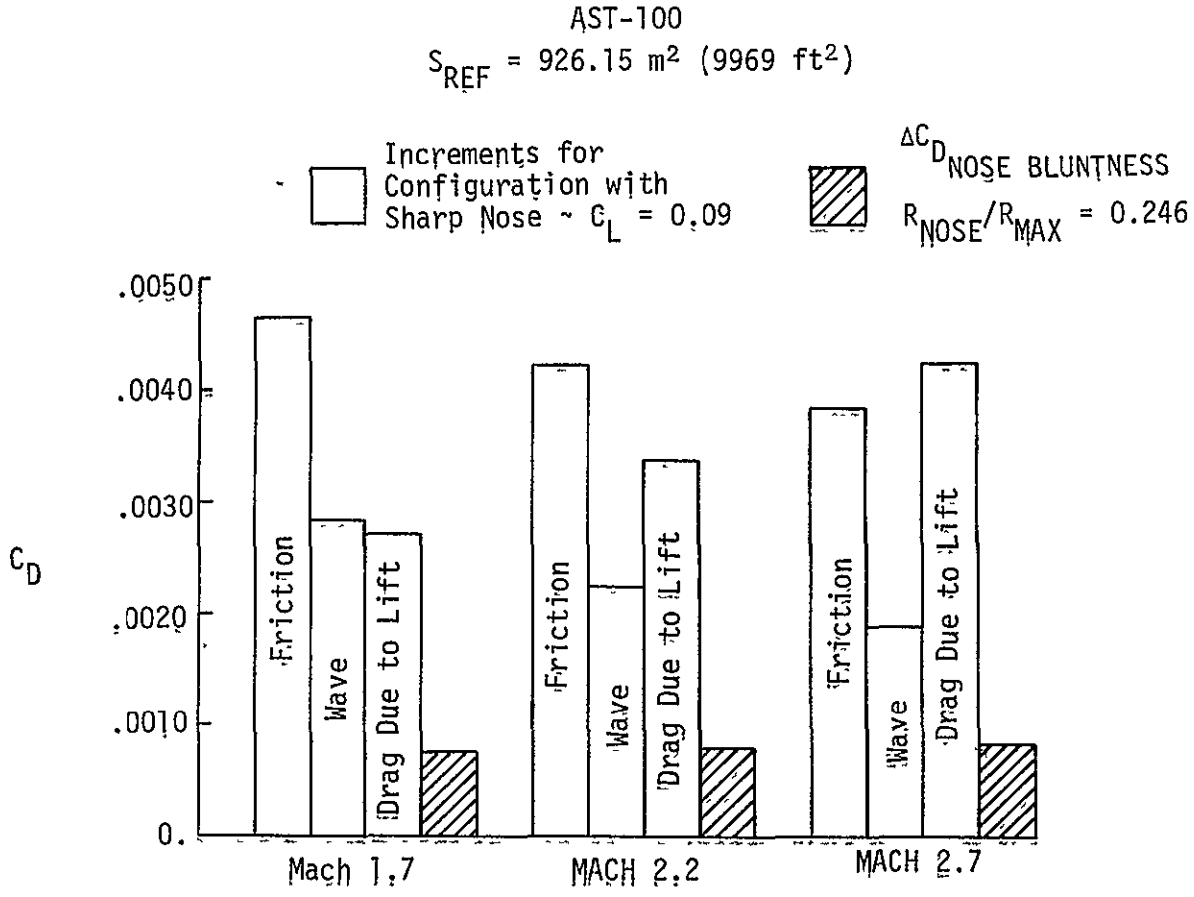

Figure 12. AST-100 Configuration Drag Build-Up

APPENDIX

Lighthill Integral Method for Axisymmetric Bodies

A method developed by M. J. Lighthill has been used to calculate body pressure distributions and the associated zero-lift wave drag coefficients for a typical sharp-nosed AST (Advanced Supersonic Technology) fuselage. The purpose of this appendix is to discuss the numerical approach to the solution of the Lighthill equation, to validate the method through correlation of results obtained for several minimum drag bodies of revolution with appropriate experimental data, and to discuss the convergence characteristics of the method. A listing of both the FORTRAN computer program written to implement the technique and output for a typical case are also included.

Lighthill Equation and Numerical Approach

The equation for the surface pressure coefficient on a body of revolution has been shown by Lighthill in reference A-1 to be

$$C_p = \frac{1}{\pi} \int_0^x \frac{U(Z)dS'(t)}{\beta R(t)} - [R'(x)]^2 \qquad \text{(A-1)}$$

where

x = body field station

$U(Z)$ = decay function

Z = position function, $= \frac{x - t}{\beta R(t)}$

t = x variable of integration

β = Mach number parameter, $= \sqrt{M_\infty^2 - 1}$

$R(t)$ = body radius at t

$S'(t)$ = first derivative of body cross-sectional area S at t

$R'(x)$ = first derivative of body radius R at x

Equation (A-1) is valid for any slender body of revolution whether it is smooth or not. It is easily evaluated numerically because the integrand is without singularities. The decay function U(Z) is shown in Figure (A-1) where the function 1/z is also presented for comparison. U(Z) is zero for $z < 0$,

unity at z = 0, and falls asymptotically to zero as $Z \to \infty$. The development of U(Z) has been presented by Lighthill in reference A-2 while reference A-1 further discusses the implementation in the present problem.

If a given body of revolution is divided into a finite number of stations [X,R(X)], equation (A-1) may be rewritten as:

$$C_P = \frac{1}{\pi} \sum_{k=1}^{k=I} \bar{U}_k \left(S'_k - S'_{k-1}\right) - \left(R'_I\right)^2 \qquad (A\text{-}2)$$

where the integral has been replaced by a summation from the first body station K = 1 to the I'th point on the body. Similarly, $dS''(t)$ has been written as the difference $S'_k - S'_{k-1}$. A mean value of the decay function on a given x-interval may be obtained using logarithms as follows:

$$\log \bar{U}_k = \frac{1}{2}\left[\log\left(\frac{U_k}{\beta R_k}\right) + \log\left(\frac{U_{k-1}}{\beta R_{k-1}}\right)\right] \qquad (A\text{-}3)$$

or,

$$\bar{U}_k = e^{\frac{1}{2}\left[\log\left(\frac{U_k}{\beta R_k}\right) + \log\left(\frac{U_{k-1}}{\beta R_{k-1}}\right)\right]} \qquad (A\text{-}4)$$

thus,

$$\bar{U}_k = \sqrt{\left(\frac{U_k}{\beta R_k}\right)\left(\frac{U_{k-1}}{\beta R_{k-1}}\right)} \qquad (A\text{-}5)$$

The use of logarithms in this development is advantageous because the function $\log [U(Z)/\beta R(t)]$ is approximately linear in Z.

The expression for numerically evaluating the pressure coefficient at a given point I on a slender body of revolution is thus:

$$C_P = \frac{1}{\pi} \sum_{k=1}^{k=I} \sqrt{\left(\frac{U_k}{\beta R_k}\right)\left(\frac{U_{k-1}}{\beta R_{k-1}}\right)} \left(S'_k - S''_{k-1}\right) - \left(R'_I\right)^2 \qquad (A\text{-}6)$$

where the last term may be evaluated simply as:

$$R'_I = \frac{R_I - R_{I-1}}{X_I - X_{I-1}} \tag{A-7}$$

Note in equation (A-6) that the radius R must always be non-zero. The solution for a given closed body must start just aft of the nose and terminate just ahead of the afterbody closure point. Let the solution begin at $X=X_1$ such that the first two body stations X_0 and X_1 define an initial cone of half-angle δ_1. The contribution of the initial cone at $X=X_1$ may be evaluated as follows: At X_0 the radius $R_0 = 0$ and

$$S'_0 = 2\pi R_0 \left(\frac{dR}{dX}\right)_0 = 0 \tag{A-8}$$

Now as $t \to X_0$ the radius $R(t) \to 0$ and $Z \to \infty$. Thus, $U(Z) \to 1/Z$:

$$U_0 = \frac{1}{Z} = \frac{\beta R_0}{X_1 - t} = \frac{\beta R_0}{X_1} \tag{A-9}$$

or,

$$\frac{U_0}{\beta R_0} = \frac{1}{X_1} \tag{A-10}$$

as $t \to X_1$, $(X_1 - t)/\beta R(t) \to 0$ and

$$U_1 = 1 \tag{A-11}$$

such that

$$\frac{U_1}{\beta R_1} = \frac{1}{\beta R_1} \tag{A-12}$$

Also,

$$S'_1 = 2\pi R_1 \left(\frac{dR}{dX}\right)_1 = 2\pi R_1 \delta_1 \tag{A-13}$$

Substituting these relations into equation (A-6) gives

$$C_{P_1} = \frac{1}{\pi}\sqrt{\left(\frac{1}{\beta R_1}\right)\left(\frac{1}{X_1}\right)}\quad (2\pi\delta_1^2 X_1) - \delta_1^2 \tag{A-14}$$

or,

$$C_{P_1} = \delta_1^2\left[\frac{2}{\sqrt{\beta\delta_1}} - 1\right] \tag{A-15}$$

where C_{P_1} is the pressure coefficient at $x = x_1$ due to the conical nose. This result compares favorably with the slender body result (reference A-3)

$$C_P = \delta_1^2\left[2\log\frac{2}{\beta\delta} - 1\right] \tag{A-16}$$

No special treatment is required if the afterbody closes. The calculation is stopped just forward of the closure point such that the neglected drag contribution is insignificant.

Once the body pressure distribution is known, the drag coefficient is calculated as

$$C_D = \frac{\pi}{2S_{REF}}\sum_{k=1}^{k=N}(R_k^2 - R_{k-1}^2)\quad(C_{P_k} + C_{P_{k-1}}) \tag{A-17}$$

where S_{REF} is the reference area and N is the total number of stations used to represent the body. Note again that insignificant drag contributions associated with the initial cone and afterbody closure point are omitted.

This technique for calculating the pressure distribution and wave drag coefficient of a slender body of revolution has been programmed for the CDC Cyber series computers using the FORTRAN Extended language. A listing of this code and output for a typical case are presented at the end of this appendix. It should be noted that the execution times for this method are very fast (on the order of a few seconds) and that the solution is inherently free of potential numerical instabilities.

Accuracy and Convergence Characteristics

Typical convergence characteristics of the Lighthill method are shown in Figure A-2. The smooth body of revolution considered has a fineness ratio of 8.0 and the freestream Mach number is 3.0. As the figure indicates, the Lighthill integral converges rapidly to the final solution and agrees quite well with the method of characteristics solution.

Three minimum drag bodies of fineness ratio 7, 10, and 13 have been studied using the Lighthill method. As shown in Figures A-3 and A-4, the predicted pressure distributions and wave drag coefficients show excellent agreement with both the method of characteristics solution and the experimental data (reference A-4) for a wide range of Mach numbers.

Results obtained for a typical closing afterbody are presented in Figure A-5. The experimental data have been obtained by William K. Abeyounis of the NASA Langley Research Center and are unpublished. Although the Lighthill theory overpredicts the afterbody pressures, the agreement is still reasonable. Note in particular that a finite pressure coefficient is obtained at the point where the solution is terminated ($x/\ell = 0.997$).

The results presented above have indicated both good accuracy and convergence characteristics of the method when applied to smooth analytic shapes. Analysis of typical area-ruled fuselages has pointed to some lack of convergence in the computed wave drag coefficient, however. As shown in Figure A-6, satisfactory convergence has not been achieved using as many as 501 points to define the body radius dsitribution. The extrapolation technique illustrated in the figure can be used to estimate the converged results as shown. The resulting wave drag variation with Mach number is also shown in Figure A-6.

In conclusion, the Lighthill technique presents a rapid method for determination of pressure distributions and wave drag coefficients for bodies of revolution in supersonic flow. Care must be taken, however, to insure that converged results are obtained.

References

A-1 Lighthill, M. J.: General Theory of High Speed Aerodynamics. Higher Approximations. Volume VI of High Speed Aerodynamics and Jet Propulsion, Ch. 8, Sec. E, W. R. Sears, ed., Princeton University Press, 1954.

A-2 Lighthill, M. J.: Supersonic Flow Past Bodies of Revolution. British R. and M. No. 2003, 1945.

A-3 Liepmann, H. W. and Roshko, A.: Elements of Gasdynamics, John Wiley and Sons, Inc., 1967.

A-4 Harris, Roy V., Jr. and Landrum, Emma Jean: Drag Characteristics of a Series of Low-Drag Bodies of Revolution at Mach Numbers from 0.6 to 4.0. NASA TN D-3163, 1965.

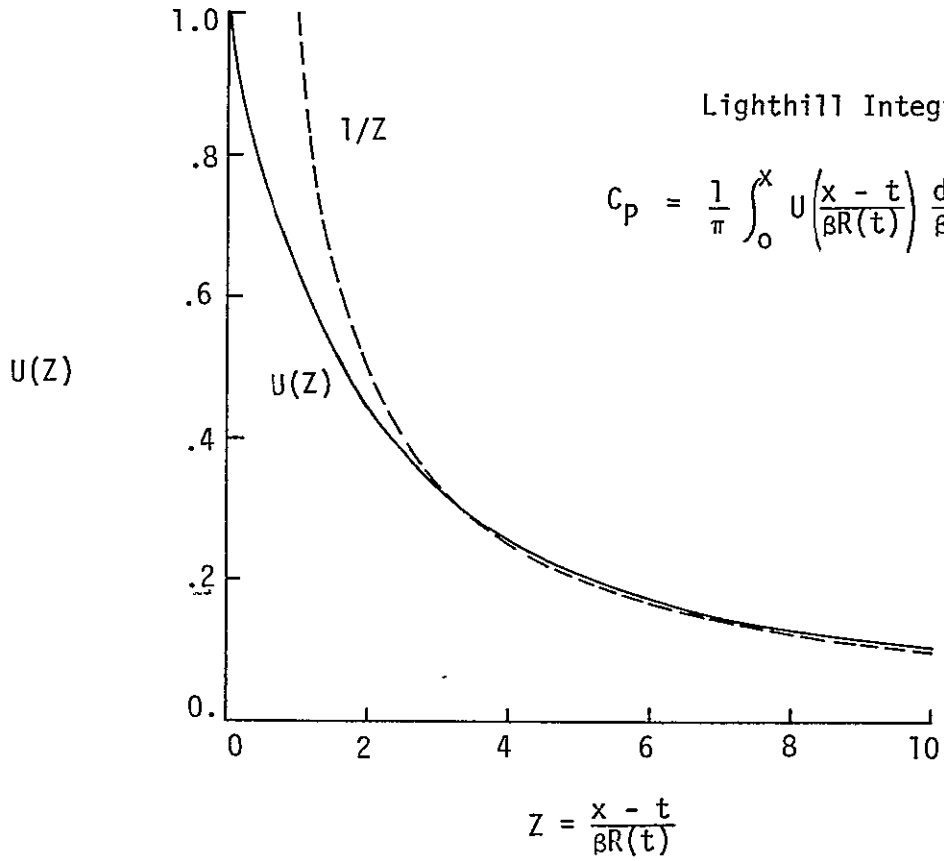

Figure A-1. Decay Function U(Z) for the Lighthill Integral

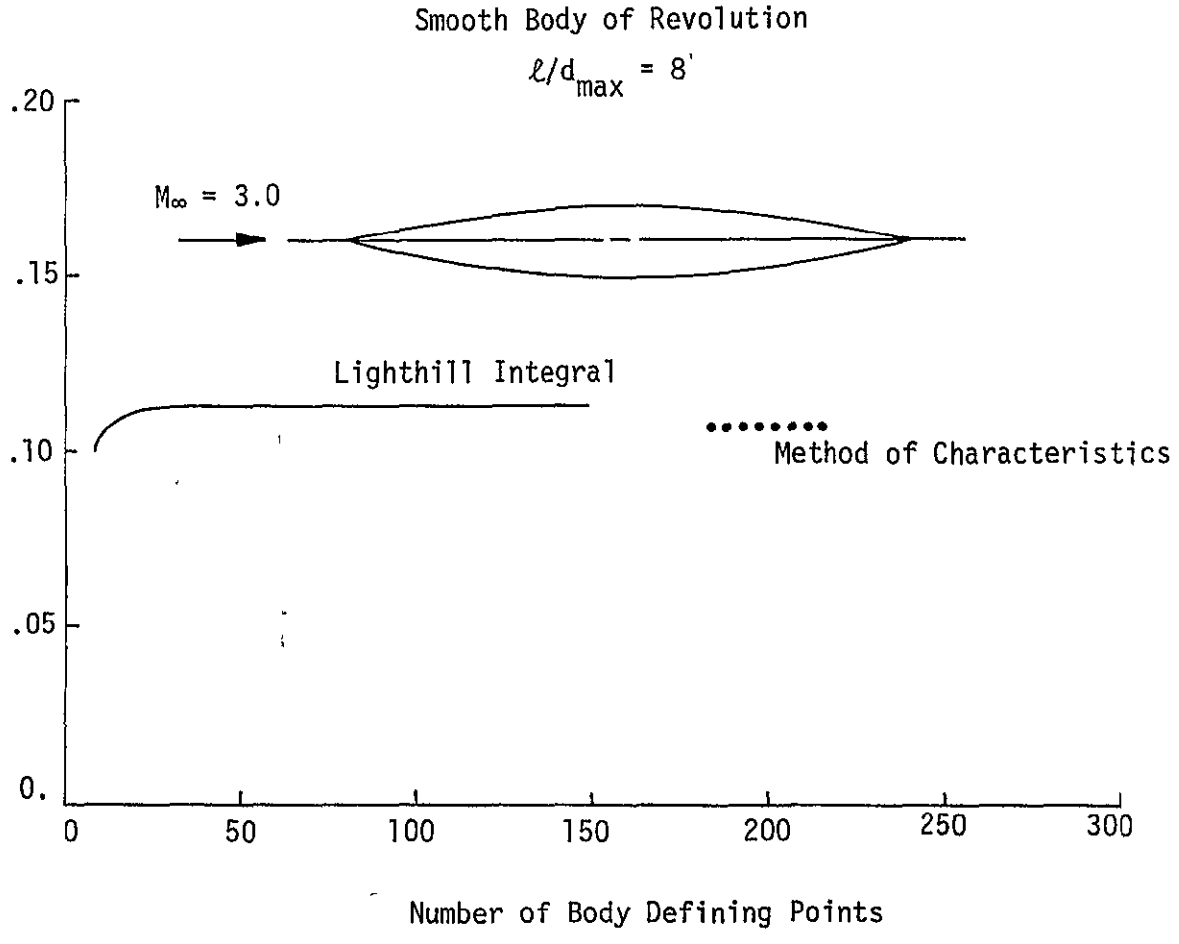

Figure A-2. Convergence Characteristics of the Lighthill Integral

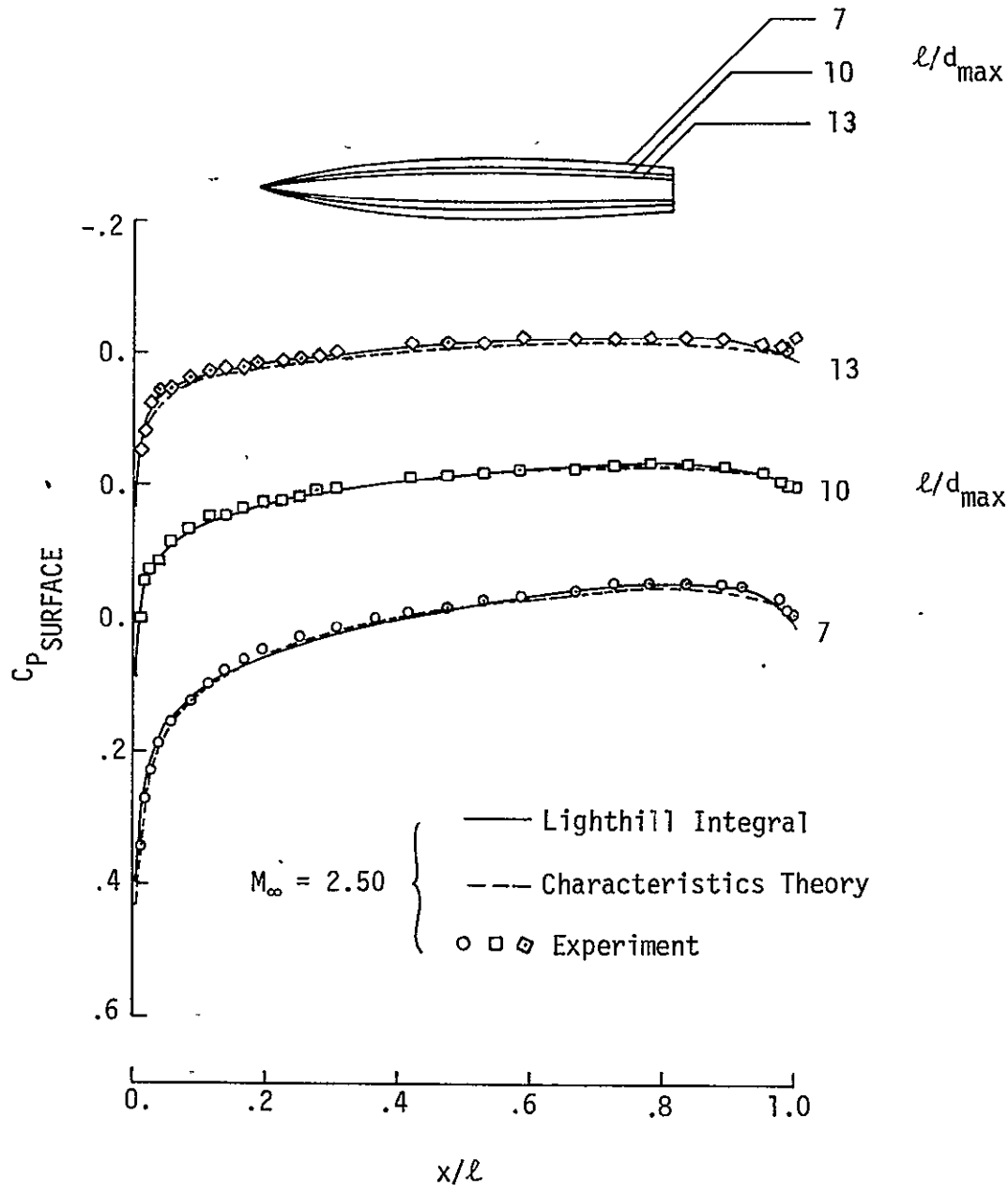

Figure A-3. Pressure Coefficient Correlation for Minimum Drag Bodies

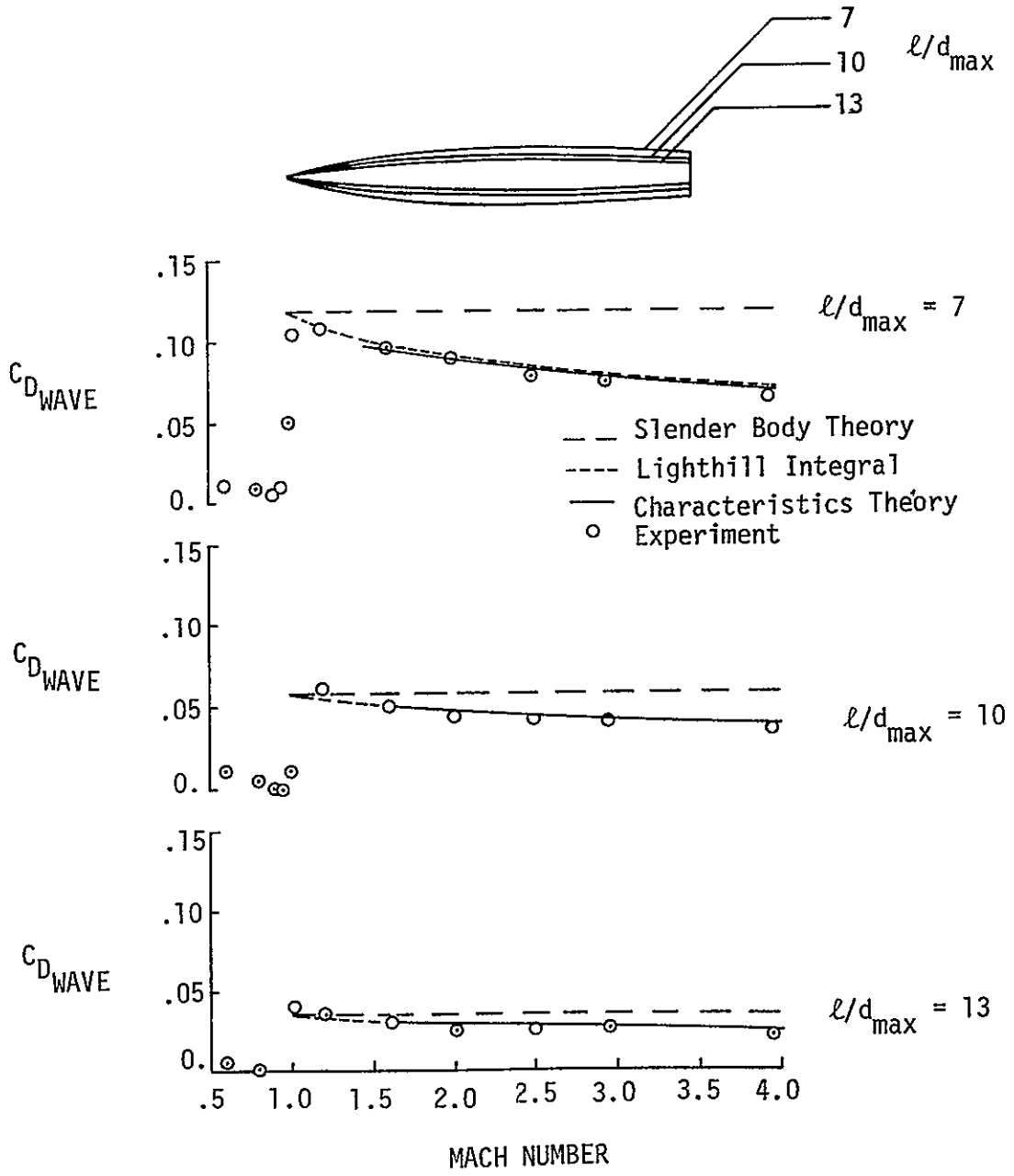

Figure A-4. Wave Drag Correlation for Minimum Drag Bodies

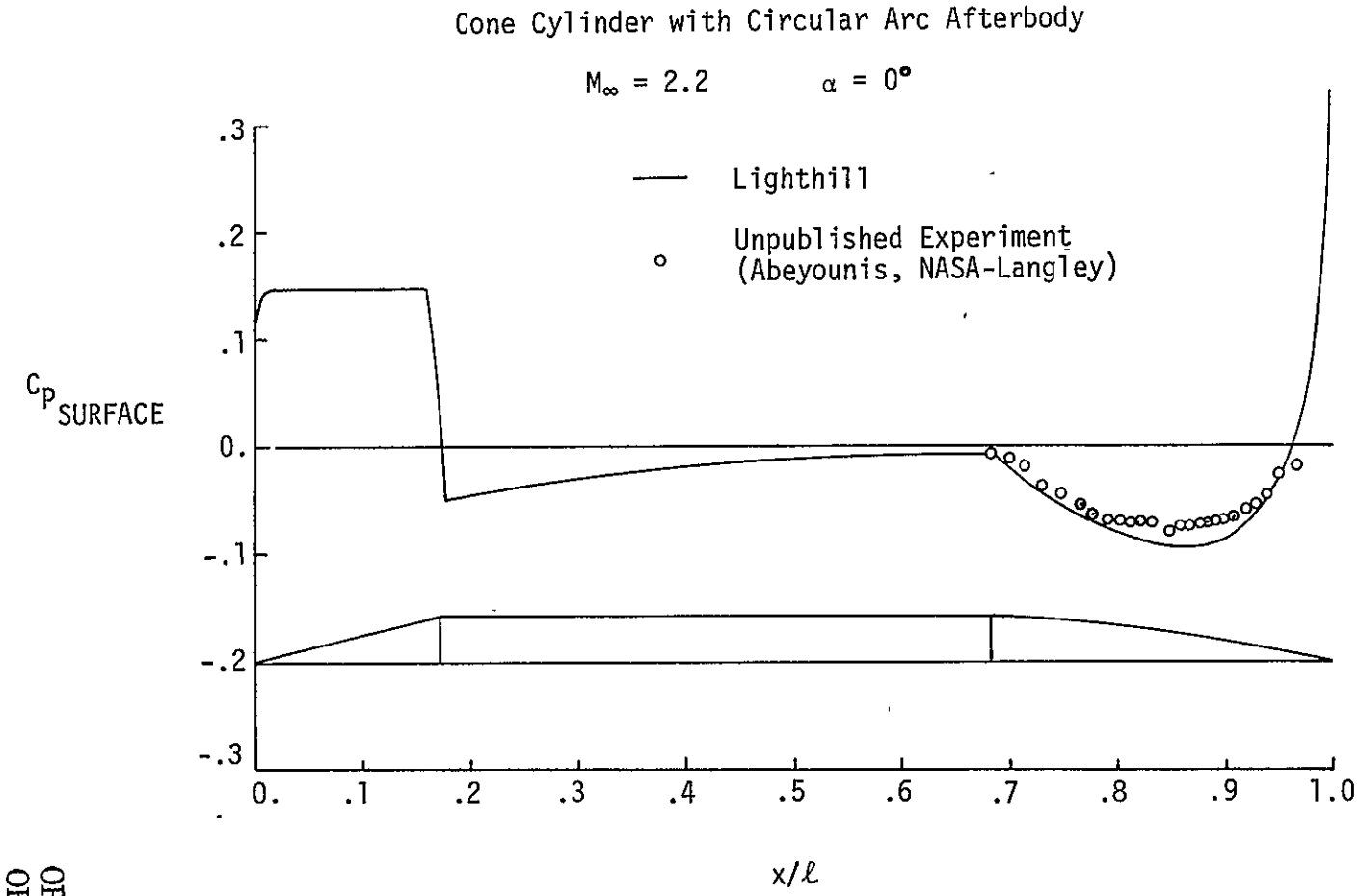

Figure A-5. Correlation of Afterbody Pressure Distributions

Slender Area-Ruled Fuselage

Lighthill Solution

S_{REF} = 926.15 m^2 (9969 ft^2)

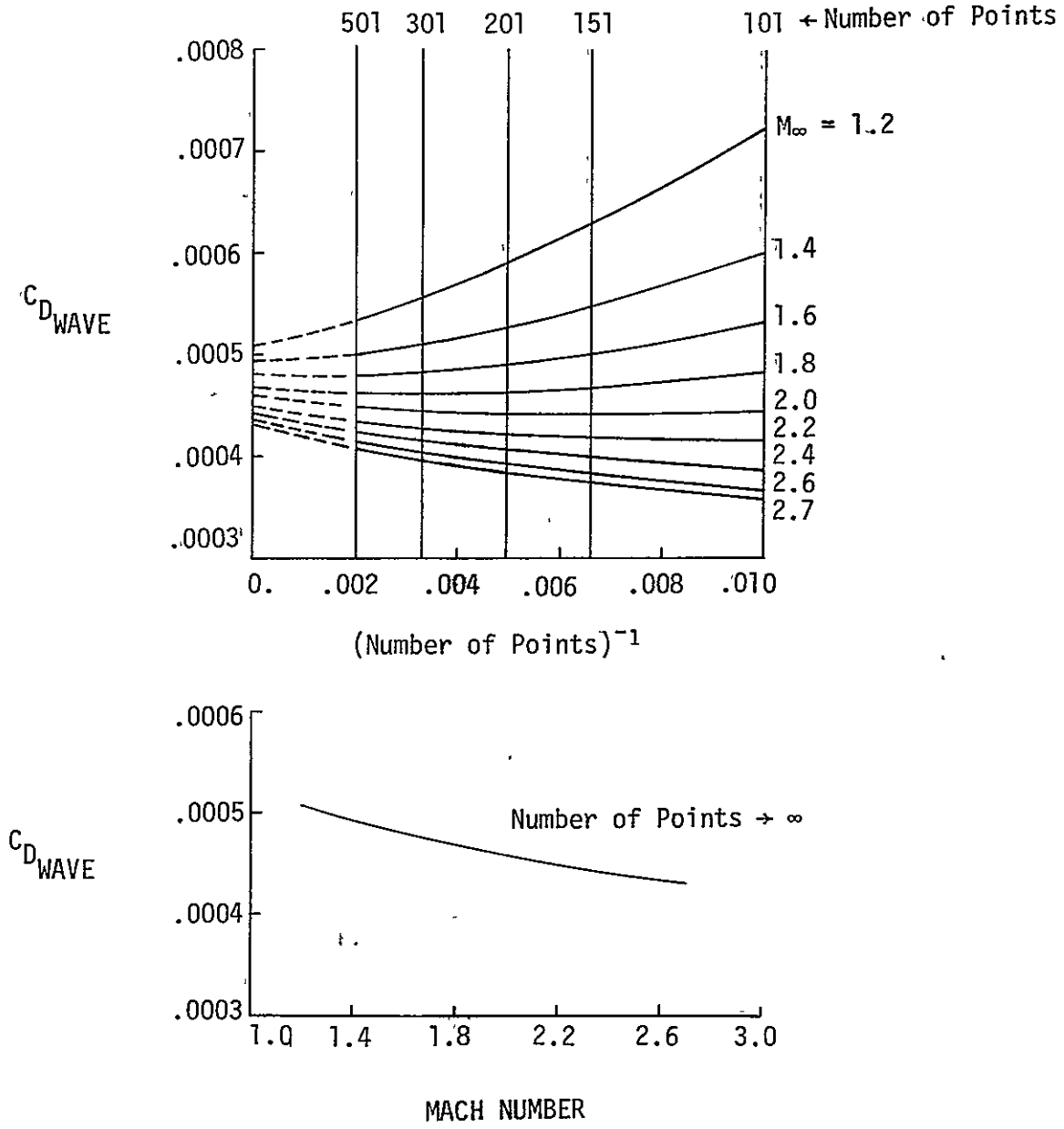

Figure A-6. Wave Drag Calculation for a Slender Area-Ruled Fuselage

```
      PROGRAM DRAG(INPUT,OUTPUT,TAPE5=INPUT,TAPE6=OUTPUT)
C
C     CALCULATES PRESSURE DISTRIBUTION AND WAVE DRAG FOR A SLENDER
C     POINTED BODY OF REVOLUTION USING THE LIGHTHILL INTEGRAL FOR
C     NON-SMOOTH BODIES
C
C
C**********************  INPUT REQUIREMENTS  ****************************
C
C     CARD 1   TITLE INFORMATION - FORMAT(8A10)
C
C     CARD 2   NMACH,NPTS - FORMAT(2I3)
C
C                   NMACH-NUMBER OF MACH NUMBERS (.LE.10)
C                   NPTS -NUMBER OF POINTS DEFINING BODY GEOMETRY
C
C     CARD 3   AM - ARRAY OF MACH NUMBERS - FORMAT(10F7.0)
C
C
C              NOTE: SUBROUTINE GEOM PROVIDES (STATION,RADIUS)
C                    DATA AND MAY BE SET UP TO COMPUTE OR
C                    READ AS REQUIRED FOR A GIVEN PROBLEM.
C
C*****************************************************************************
      DIMENSION X(501),R(501),S(501),RP(501),SP(501),CP(501)
      DIMENSION ABC(8),AM(10)
C
C     READ TITLE
C
  500 READ(5,10) ABC
   10 FORMAT(8A10)
C
      IF(EOF(5)) 20,30
   20 STOP
   30 CONTINUE
C
C     READ NMACH,NPTS
C
      READ(5,40) NMACH,NPTS
   40 FORMAT(2I3)
C
C     READ ARRAY OF MACH NUMBERS
C
      READ(5,50) (AM(I),I=1,NMACH)
   50 FORMAT(10F7.0)
C
C     GENERATE OR READ BODY GEOMETRY
C
      CALL GEOM(X,R,S,SREF,NPTS)
C
C     CALCULATE BODY RADIUS AND AREA DERIVATIVES - OMIT LAST BODY
C     STATION IF R(NPTS)=0.
C
      IF(R(NPTS).EQ.0.) NPTS=NPTS-1
C
```

```
      PI=3.141592654
      RP(1)=R(1)/X(1)
      SP(1)=2.*PI*R(1)*RP(1)
C
      DO 60 K=2,NPTS
      KK=K-1
      DELX=X(K)-X(KK)
      RP(K)=(R(K)-R(KK))/DELX
      SP(K)=2.*PI*R(K)*RP(K)
   60 CONTINUE
C
C     MACH NUMBER LOOP FOR GIVEN (X,R) GEOMETRY
C
      DO 1000 L=1,NMACH
C
      BETA=SQRT(AM(L)*AM(L)-1.)
      CPVAC=-2./(1.4*AM(L)*AM(L))
C
C     CALCULATE PRESSURE DISTRIBUTION AND WAVE DRAG
C
      CALL CPDRAG(BETA,X,R,RP,SP,NPTS,SREF,CP,CDO)
C
C     WRITE OUTPUT FOR CURRENT MACH NUMBER
C
      CALL OUT(X,R,S,RP,SP,CP,NPTS,CDO,SREF,AM(L),ABC,CPVAC)
C
 1000 CONTINUE
C
C     NEXT GEOMETRY
C
      GO TO 500
C
      END
```

```
      SUBROUTINE GEOM(X,R,S,SREF,NPTS)
C
C     TO PROVIDE THE REQUIRED GEOMETRY DATA - THIS ROUTINE
C     MUST EITHER CALCULATE,READ,OR EXPLICITLY DEFINE THE
C     (STATION,RADIUS) DATA AT NPTS POINTS
C
C     X(1) AND R(1) MUST BE GREATER THAN ZERO
C
      DIMENSION X(NPTS),R(NPTS),S(NPTS)
C
C     GENERATE HAACK-ADAMS BODY (L/DMAX=13)  NASA TN D-3163
C
      PI=3.141592654
      RMAX=1.385
      XL=36.
      XINC=.005
      X(1)=.001
      X(2)=.005
C
      DO 10 I=3,NPTS
      X(I)=X(I-1)+XINC
   10 CONTINUE
C
      DO 20 I=1,NPTS
      XDEL=2.*X(I)-1.
      T1=.707*(1.-XDEL*XDEL)**1.5
      T2=.16934*XDEL*SQRT(1.-XDEL*XDEL)
      T3=.16934*ACOS(-XDEL)
C
      R(I)=SQRT(T1+T2+T3)*RMAX
      S(I)=PI*R(I)*R(I)
      X(I)=X(I)*XL
C
   20 CONTINUE
C
C     DEFINE REFERENCE AREA
C
      SREF=PI*RMAX*RMAX
C
      RETURN
      END
```

```
      SUBROUTINE CPDRAG(BETA,X,R,RP,SP,NPTS,SREF,CP,CDO)
C
C     TO COMPUTE THE BODY PRESSURE DISTRIBUTION AND
C     WAVE DRAG COEFFICIENT USING THE LIGHTHILL INTEGRAL
C
      DIMENSION X(NPTS),R(NPTS),RP(NPTS),SP(NPTS),CP(NPTS)
      DIMENSION PSIT(36),UTAB(36)
      DATA PSIT/0.,.2,.4,.6,.8,1.,1.2,1.4,1.6,1.8,2.,2.2,2.4,2.6,2.8,3.0
     *,3.2,3.4,3.6,3.8,4.,4.4,4.8,5.2,5.6,6.,6.4,6.8,7.2,7.6,8.,8.4,8.8,
     *9.2,9.6,10./
      DATA UTAB/1.,.90703,.82646,.75621,.69462,.64034,.59229,.54960,
     *.51149,.47737,.44672,.41907,.39408,.37140,.35080,.33201,.31483,
     *.29909,.28464,.27134,.25906,.23721,.21840,.20209,.18785,.17534,
     *.16428,.15445,.14567,.13778,.13068,.12424,.11839,.11304,.10815,
     *.10366/
C
      PI=3.141592654
C
C     PRESSURE COEFFICIENT AT FIRST BODY STATION
C     DUE TO INITIAL CONE
C
      CP(1)=RP(1)*RP(1)*(2./SQRT(BETA*RP(1))-1.)
C
      DO 10 I=2,NPTS
      ULAST=1./X(I)
      SUM2=0.
      DO 20 K=1,I
      PSI=(X(I)-X(K))/(BETA*R(K))
      IF(PSI.GT.10.) GO TO 30
      CALL FTLUP(PSI,U,1,36,PSIT,UTAB)
      GO TO 40
   30 U=1./PSI
   40 CONTINUE
C
      IF(K.EQ.1) SS=0.
      IF(K.GT.1) SS=SP(K-1)
      SUM2=SUM2+SQRT(ULAST*U/(BETA*R(K)))*(SP(K)-SS)/PI
      ULAST=U/(BETA*R(K))
   20 CONTINUE
C
      CP(I)=SUM2-RP(I)*RP(I)
C
   10 CONTINUE
C
C     COMPUTE WAVE DRAG
C
      DOQ=CP(1)*PI*R(1)*R(1)
C
      DO 50 I=2,NPTS
      DOQ=DOQ+PI*(R(I)*R(I)-R(I-1)*R(I-1))/2.*(CP(I)+CP(I-1))
   50 CONTINUE
C
      CDO=DOQ/SREF
C
      RETURN
      END
```

```
      SUBROUTINE OUT(X,R,S,RP,SP,CP,NPTS,CDO,SREF,XM,ABC,CPVAC)
C
C     TO WRITE GEOMETRY AND AERODYNAMIC DATA
C
      DIMENSION X(NPTS),R(NPTS),S(NPTS),RP(NPTS),SP(NPTS),CP(NPTS)
      DIMENSION ABC(8)
C
      WRITE(6,10) ABC,XM,CPVAC
   10 FORMAT(1H1,1X,8A10,//,13X,7HMACH = ,F10.7,
     *10X,12HVACUUM CP = ,F10.7,
     *//,8X,1HX,15X,1HR,15X,
     *1HS,15X,5HDR/DX,11X,5HDS/DX,11X,2HCP,//)
C
      DO 20 I=1,NPTS
      WRITE(6,30) X(I),R(I),S(I),RP(I),SP(I),CP(I)
   30 FORMAT(6F16.8)
   20 CONTINUE
C
      WRITE(6,40) XM,CDO,SREF
   40 FORMAT(//,5X,11HMACH NO. = ,F10.6,5X,10HCD WAVE = ,F10.6,5X,7HSREF
     * = ,F10.5)
C
      RETURN
      END
```

```
      SUBROUTINE FTLUP (X,Y,M,N,VARI,VARD)
*********DOCUMENT DATE  7/7/69     SUBROUTINE REVISED  7/7/69  *********
*        MODIFICATION OF LIBRARY INTERPOLATION SUBROUTINE  FTLUP
      DIMENSION VARI(N),VARD(N),V(3),YY(2)
      DIMENSION II(43)
*
*      INITIALIZE ALL INTERVAL POINTERS TO -1.0   FOR MONOTONICITY CHECK
      DATA (II(J),J=1,43)/43*-1/
      MA=IABS(M)
*
*            ASSIGN INTERVAL POINTER FOR GIVEN VARI TABLE
*      THE SAME POINTER WILL BE USED ON A GIVEN VARI TABLE EVERY TIME
      LI=MOD(LOCF(VARI(1)),43)+1
      I=II(LI)
      IF (I.GE.0) GO TO 10
      IF (N.LT.2) GO TO 10
*
* MONOTONICITY CHECK
      IF (VARI(2)-VARI(1)) 1,1,3
*  ERROR IN MONOTONICITY
    2 K=LOCF (VARI(1))
      PRINT 102,J,K,(VARI(J),J=1,N),(VARD(J),J=1,N)
  102 FORMAT (1H1,* TABLE BELOW OUT OF ORDER FOR FTLUP  AT POSITION  *
     1,I5,/* X TABLE IS STORED IN LOCATION *,O6,//(8G15.8))
      STOP
```

```
*  MONOTONIC DECREASING
    1 DO 5 J=2,N
      IF (VARI(J)-VARI(J-1))5,2,2
    5 CONTINUE
      GO TO 10
*  MONOTONIC INCREASING
    3 DO 6 J=2,N
      IF (VARI(J)-VARI(J-1))2,2,6
    6 CONTINUE
*
* INTERPOLATION
   10 IF (I.LE.0) I=1
      IF (I.GE.N) I=N-1
      IF (N.LE.1) GO TO 8
      IF (MA.NE.0) GO TO 99
*  ZERO ORDER
    8 Y=VARD(1)

      GO TO 800
*  LOCATE I INTERVAL (X(I).LE.X.LT.X(I+1))
   99 IF ((VARI(I)-X)*(VARI(I+1)-X)) 61,61,40
*  IN GIVES DIRECTION FOR SEARCH OF INTERVALS
   40 IN=SIGN(1.0,(VARI(I+1)-VARI(I))*(X-VARI(I)))
*  IF X OUTSIDE ENDPOINTS, EXTRAPOLATE FROM END INTERVAL
   41 IF ((I+IN).LE.0) GO TO 61
      IF ((I+IN).GE.N) GO TO 61
      I=I+IN
      IF ((VARI(I)-X)*(VARI(I+1)-X)) 61,61,41
   61 IF (MA.EQ.2) GO TO 200
*
* FIRST ORDER
      Y=(VARD(I)*(VARI(I+1)-X)-VARD(I+1)*(VARI(I)-X))/(VARI(I+1)-VARI(I)
     1   )
      GO TO 800
*
* SECOND ORDER
  200 IF (N.EQ.2) GO TO 2
      IF (I.EQ.(N-1)) GO TO 209
      IF (I.EQ.1) GO TO 201
*  PICK THIRD POINT
      SK= VARI(I+1)-VARI(I)
      IF ((SK*(X-VARI(I-1))).LT.(SK*(VARI(I+2)-X))) GO TO 209
  201 L=I
      GO TO 702
  209 L=I-1
  702 V(1)=VARI(L)-X
      V(2)=VARI(L+1)-X
      V(3)=VARI(L+2)-X
      YY(1)=(VARD(L)*V(2)-VARD(L+1)*V(1))/(VARI(L+1)-VARI(L))
      YY(2)=(VARD(L+1)*V(3)-VARD(L+2)*V(2))/(VARI(L+2)-VARI(L+1))
      Y=(YY(1)*V(3)-YY(2)*V(1))/(VARI(L+2)-VARI(L))
  800 II(LI)=I
      RETURN
      END
```

HAACK-ADAMS BODY (NASA TN D-3163) L/DMAX=13

MACH = 2.5000000 VACUUM CP = -.2285714

X	R	S	DR/DX	DS/DX	CP
.03600000	.01993350	.00124829	.55370823	.06934966	.23779907
.18000000	.06647351	.01388184	.32319454	.13498717	.17448230
.36000000	.11141983	.03900092	.24970176	.17480907	.12797003
.54000000	.15051021	.07116751	.21716877	.20537292	.10518836
.72000000	.18612239	.10882962	.19784548	.23136871	.09322190
.90000000	.21928216	.15106243	.18422994	.25381786	.08463309
1.08000000	.25055605	.19722396	.17374384	.27352320	.07795337
1.26000000	.28030064	.24683006	.16524769	.29103107	.07254449
1.44000000	.30875963	.29949592	.15810554	.30672380	.06798630
1.62000000	.33610943	.35490431	.15194334	.32087969	.06405892
1.80000000	.36248320	.41278664	.14652090	.33370853	.06025137
1.98000000	.38798475	.47291074	.14167529	.34537320	.05727428
2.16000000	.41269716	.53507275	.13729118	.35600328	.05456474
2.34000000	.43668830	.59909126	.13328409	.36570403	.05209337
2.52000000	.46001457	.66480311	.12959039	.37456244	.04983358
2.70000000	.48272354	.73206027	.12616099	.38265152	.04772650
2.88000000	.50485586	.80072739	.12295733	.39003332	.04577377
3.06000000	.52644660	.87067992	.11994855	.39676120	.04380332
3.24000000	.54752633	.94180261	.11710959	.40288150	.04210186
3.42000000	.56812190	1.01398828	.11441984	.40843479	.04048905
3.60000000	.58825709	1.08713684	.11186217	.41345693	.03895726
3.78000000	.60795308	1.16115448	.10942218	.41797981	.03750548
3.96000000	.62722886	1.23595296	.10708766	.42203196	.03612562
4.14000000	.64610153	1.31144903	.10484817	.42563907	.03471415
4.32000000	.66458658	1.38756395	.10269471	.42882442	.03345510
4.50000000	.68269809	1.46422307	.10061949	.43160917	.03224592
4.68000000	.70044891	1.54135546	.09861569	.43401263	.03108512
4.86000000	.71785084	1.61889356	.09667736	.43605257	.02996475
5.04000000	.73491469	1.69677296	.09479921	.43774531	.02881657
5.22000000	.75165048	1.77493212	.09297657	.43910595	.02777506
5.40000000	.76806743	1.85331214	.09120529	.44014851	.02676532
5.58000000	.78417412	1.93185661	.08948164	.44088601	.02578970
5.76000000	.79997854	2.01051142	.08780229	.44133062	.02483875
5.94000000	.81548810	2.08922458	.08616423	.44149370	.02386562
6.12000000	.83070975	2.16794615	.08456474	.44138592	.02297403
6.30000000	.84564999	2.24662803	.08300134	.44101731	.02210170

X	R	S	DR/DX	DS/DX	CP
6.48000000	.86031492	2.32522391	.08147181	.44039733	.02125508
6.66000000	.87471025	2.40368917	.07997408	.43953489	.02042653
6.84000000	.88884139	2.48198075	.07850639	.43843844	.01957971
7.02000000	.90271340	2.56005709	.07706673	.43711600	.01879361
7.20000000	.91633109	2.63787804	.07565381	.43557517	.01802309
7.38000000	.92969898	2.71540481	.07426609	.43382318	.01726964
7.56000000	.94282138	2.79259988	.07290221	.43186695	.01653169
7.74000000	.95570235	2.86942698	.07156094	.42971304	.01578080
7.92000000	.96834575	2.94585098	.07024112	.42736777	.01507318
8.10000000	.98075525	3.02183787	.06894170	.42483716	.01438148
8.28000000	.99293436	3.09735474	.06766167	.42212700	.01370177
8.46000000	1.00488638	3.17236967	.06640011	.41924283	.01303404
8.64000000	1.01661449	3.24685175	.06515616	.41619001	.01235650
8.82000000	1.02812171	3.32077101	.06392901	.41297365	.01171281
9.00000000	1.03941093	3.39409840	.06271789	.40959873	.01108255
9.18000000	1.05048491	3.46680574	.06152211	.40607001	.01046145
9.36000000	1.06134629	3.53886570	.06034100	.40239211	.00983003
9.54000000	1.07199759	3.61025180	.05917393	.39856951	.00923143
9.72000000	1.08244125	3.68093832	.05802031	.39460651	.00864058
9.90000000	1.09267958	3.75090032	.05687959	.39050731	.00806040
10.08000000	1.10271480	3.82011362	.05575125	.38627597	.00748769
10.26000000	1.11254906	3.88855474	.05463479	.38191642	.00690721
10.44000000	1.12218442	3.95620093	.05352975	.37743252	.00635313
10.62000000	1.13162284	4.02303010	.05243568	.37282797	.00580667
10.80000000	1.14086623	4.08902084	.05135217	.36810642	.00526767
10.98000000	1.14991642	4.15415237	.05027882	.36327139	.00472271
11.16000000	1.15877516	4.21840457	.04921525	.35832634	.00419875
11.34000000	1.16744416	4.28175791	.04816111	.35327462	.00368287
11.52000000	1.17592505	4.34419346	.04711605	.34811953	.00317380
11.70000000	1.18421941	4.40569290	.04607976	.34286427	.00265873
11.88000000	1.19232875	4.46623846	.04505192	.33751199	.00216380
12.06000000	1.20025456	4.52581295	.04403225	.33206576	.00167461
12.24000000	1.20799824	4.58439971	.04302046	.32652859	.00119136
12.42000000	1.21556117	4.64198264	.04201629	.32090344	.00070445
12.60000000	1.22294468	4.69854615	.04101948	.31519320	.00023429
12.78000000	1.23015004	4.75407517	.04002980	.30940072	-.00023048
12.96000000	1.23717850	4.80855516	.03904700	.30352879	-.00068892
13.14000000	1.24403126	4.86197206	.03807087	.29758014	-.00115166
13.32000000	1.25070947	4.91431230	.03710119	.29155749	-.00159905
13.50000000	1.25721427	4.96556280	.03613777	.28546348	-.00204071
13.68000000	1.26354675	5.01571095	.03518041	.27930074	-.00247773
13.86000000	1.26970795	5.06474462	.03422892	.27307183	-.00291756
14.04000000	1.27569891	5.11265214	.03328312	.26677931	-.00334344

X	R	S	DR/DX	DS/DX	CP
14.22000000	1.28152063	5.15942229	.03234285	.26042566	-.00376470
14.40000000	1.28717406	5.20504428	.03140794	.25401338	-.00418118
14.58000000	1.29266014	5.24950781	.03047823	.24754489	-.00459952
14.76000000	1.29797978	5.29280298	.02955357	.24102262	-.00500601
14.94000000	1.30313387	5.33492034	.02863383	.23444895	-.00540770
15.12000000	1.30812326	5.37585085	.02771885	.22782624	-.00580471
15.30000000	1.31294880	5.41558593	.02680851	.22115682	-.00620333
15.48000000	1.31761128	5.45411737	.02590268	.21444301	-.00659107
15.66000000	1.32211150	5.49143743	.02500124	.20768710	-.00697401
15.84000000	1.32645023	5.52753874	.02410407	.20089137	-.00735828
16.02000000	1.33062823	5.56241435	.02321107	.19405806	-.00773264
16.20000000	1.33464621	5.59605773	.02232211	.18718942	-.00810216
16.38000000	1.33850489	5.62846273	.02143711	.18028765	-.00846753
16.56000000	1.34220496	5.65962361	.02055595	.17335498	-.00883372
16.74000000	1.34574710	5.68953504	.01967856	.16639359	-.00919060
16.92000000	1.34913197	5.71819206	.01880483	.15940565	-.00954326
17.10000000	1.35236021	5.74559013	.01793468	.15239334	-.00989612
17.28000000	1.35543246	5.77172506	.01706804	.14535882	-.01024053
17.46000000	1.35834932	5.79659310	.01620482	.13830424	-.01058068
17.64000000	1.36111141	5.82019084	.01534494	.13123173	-.01091665
17.82000000	1.36371932	5.84251529	.01448835	.12414343	-.01125225
18.00000000	1.36617361	5.86356383	.01363496	.11704147	-.01157985
18.18000000	1.36847486	5.88333423	.01278473	.10992798	-.01190341
18.36000000	1.37062363	5.90182464	.01193758	.10280507	-.01222596
18.54000000	1.37262045	5.91903359	.01109347	.09567486	-.01254112
18.72000000	1.37446587	5.93495999	.01025234	.08853948	-.01285234
18.90000000	1.37616042	5.94960316	.00941415	.08140103	-.01315940
19.08000000	1.37770461	5.96296276	.00857884	.07426163	-.01346522
19.26000000	1.37909896	5.97503886	.00774638	.06712340	-.01376427
19.44000000	1.38034397	5.98583192	.00691673	.05998846	-.01405903
19.62000000	1.38144014	5.99534275	.00608985	.05285894	-.01435216
19.80000000	1.38238797	6.00357258	.00526572	.04573696	-.01463871
19.98000000	1.38318795	6.01052301	.00444430	.03862467	-.01492108
20.16000000	1.38384055	6.01619603	.00362558	.03152419	-.01520115
20.34000000	1.38434627	6.02059401	.00280954	.02443769	-.01547506
20.52000000	1.38470558	6.02371972	.00199616	.01736732	-.01574472
20.70000000	1.38491896	6.02557632	.00118543	.01031525	-.01601000
20.88000000	1.38498688	6.02616737	.00037734	.00328366	-.01627290
21.06000000	1.38490982	6.02549680	-.00042811	-.00372525	-.01652971
21.24000000	1.38468825	6.02356898	-.00123092	-.01070927	-.01678219
21.42000000	1.38432266	6.02038864	-.00203107	-.01766619	-.01703163
21.60000000	1.38381352	6.01596095	-.00282857	-.02459376	-.01727528
21.78000000	1.38316130	6.01029147	-.00362340	-.03148973	-.01751424

X	R	S	DR/DX	DS/DX	CP
21.96000000	1.38236651	6.00338615	-.00441553	-.03835181	-.01774974
22.14000000	1.38142962	5.99525141	-.00520494	-.04517772	-.01797955
22.32000000	1.38035113	5.98589403	-.00599160	-.05196512	-.01820446
22.50000000	1.37913155	5.97532126	-.00677546	-.05871169	-.01842569
22.68000000	1.37777138	5.96354074	-.00755650	-.06541504	-.01864130
22.86000000	1.37627114	5.95056056	-.00833465	-.07207279	-.01885201
23.04000000	1.37463137	5.93638926	-.00910987	-.07868250	-.01905828
23.22000000	1.37285259	5.92103581	-.00988208	-.08524174	-.01925893
23.40000000	1.37093537	5.90450963	-.01065123	-.09174799	-.01945433
23.58000000	1.36888027	5.88682058	-.01141723	-.09819875	-.01964479
23.76000000	1.36668787	5.86797902	-.01217999	-.10459146	-.01982960
23.94000000	1.36435877	5.84799574	-.01293943	-.11092352	-.02000878
24.12000000	1.36189359	5.82688204	-.01369544	-.11719229	-.02018279
24.30000000	1.35929297	5.80464968	-.01444791	-.12339508	-.02035090
24.48000000	1.35655756	5.78131092	-.01519671	-.12952918	-.02051321
24.66000000	1.35368805	5.75687853	-.01594171	-.13559180	-.02066953
24.84000000	1.35068516	5.73136578	-.01668277	-.14158011	-.02081977
25.02000000	1.34754960	5.70478647	-.01741974	-.14749123	-.02096369
25.20000000	1.34428217	5.67715493	-.01815243	-.15332222	-.02110102
25.38000000	1.34088364	5.64848603	-.01888068	-.15907008	-.02123204
25.56000000	1.33735487	5.61879520	-.01960427	-.16473173	-.02135618
25.74000000	1.33369673	5.58809843	-.02032301	-.17030404	-.02147325
25.92000000	1.32991014	5.55641230	-.02103665	-.17578379	-.02158351
26.10000000	1.32599604	5.52375399	-.02174496	-.18116770	-.02168643
26.28000000	1.32195546	5.49014127	-.02244767	-.18645239	-.02178134
26.46000000	1.31778945	5.45559255	-.02314449	-.19163440	-.02186890
26.64000000	1.31349913	5.42012689	-.02383511	-.19671018	-.02194834
26.82000000	1.30908568	5.38376400	-.02451921	-.20167607	-.02201901
27.00000000	1.30455032	5.34652429	-.02519642	-.20652831	-.02208175
27.18000000	1.29989437	5.30842884	-.02586637	-.21126302	-.02213557
27.36000000	1.29511922	5.26949949	-.02652865	-.21587621	-.02217964
27.54000000	1.29022631	5.22975880	-.02718281	-.22036374	-.02221494
27.72000000	1.28521720	5.18923013	-.02782838	-.22472137	-.02223962
27.90000000	1.28009353	5.14793762	-.02846485	-.22894467	-.02225487
28.08000000	1.27485703	5.10590624	-.02909168	-.23302906	-.02225953
28.26000000	1.26950954	5.06316184	-.02970826	-.23696982	-.02225226
28.44000000	1.26405302	5.01973114	-.03031397	-.24076200	-.02223468
28.62000000	1.25848956	4.97564182	-.03090812	-.24440047	-.02220515
28.80000000	1.25282137	4.93092250	-.03148997	-.24787991	-.02216227
28.98000000	1.24705079	4.88560284	-.03205874	-.25119473	-.02210762
29.16000000	1.24118035	4.83971353	-.03261357	-.25433910	-.02203949
29.34000000	1.23521271	4.79328640	-.03315354	-.25730694	-.02195619
29.52000000	1.22915074	4.74635442	-.03367765	-.26009184	-.02185930

X	R	S	DR/DX	DS/DX	CP
29.70000000	1.22299747	4.69895180	-.03418482	-.26268709	-.02174585
29.88000000	1.21675617	4.65111401	-.03467390	-.26508562	-.02161759
30.06000000	1.21043031	4.60287790	-.03514364	-.26727996	-.02147246
30.24000000	1.20402363	4.55428175	-.03559267	-.26926223	-.02130822
30.42000000	1.19754012	4.50536536	-.03601952	-.27102408	-.02112679
30.60000000	1.19098405	4.45617013	-.03642260	-.27255663	-.02092448
30.78000000	1.18436002	4.40673921	-.03680017	-.27385044	-.02070287
30.96000000	1.17767296	4.35711755	-.03715035	-.27489541	-.02045944
31.14000000	1.17092816	4.30735210	-.03747109	-.27568076	-.02019168
31.32000000	1.16413133	4.25749189	-.03776015	-.27619486	-.01990098
31.50000000	1.15728861	4.20758825	-.03801510	-.27642523	-.01958318
31.68000000	1.15040663	4.15769496	-.03823326	-.27635832	-.01923943
31.86000000	1.14349252	4.10786847	-.03841171	-.27597947	-.01886678
32.04000000	1.13655402	4.05816815	-.03854723	-.27527266	-.01846167
32.22000000	1.12959949	4.00865654	-.03863628	-.27422036	-.01802505
32.40000000	1.12263800	3.95939970	-.03867497	-.27280326	-.01755149
32.58000000	1.11567938	3.91046758	-.03865895	-.27100002	-.01704184
32.76000000	1.10873437	3.86193441	-.03858342	-.26878688	-.01649151
32.94000000	1.10181463	3.81387928	-.03844299	-.26613721	-.01589577
33.12000000	1.09493293	3.76638672	-.03823165	-.26302100	-.01525416
33.30000000	1.08810327	3.71954745	-.03794258	-.25940410	-.01455936
33.48000000	1.08134102	3.67345927	-.03756805	-.25524735	-.01381016
33.66000000	1.07466316	3.62822820	-.03709922	-.25050536	-.01299929
33.84000000	1.06808851	3.58396992	-.03652586	-.24512495	-.01211873
34.02000000	1.06163802	3.54081147	-.03583600	-.23904294	-.01116453
34.20000000	1.05533523	3.49889370	-.03501551	-.23218318	-.01012395
34.38000000	1.04920671	3.45837430	-.03404732	-.22445222	-.00898956
34.56000000	1.04328283	3.41943215	-.03291049	-.21573283	-.00774346
34.74000000	1.03759868	3.38227330	-.03157858	-.20587416	-.00637143
34.92000000	1.03219559	3.34713997	-.03001717	-.19467565	-.00484739
35.10000000	1.02712328	3.31432446	-.02817949	-.18185931	-.00313552
35.28000000	1.02244361	3.28419245	-.02599822	-.16701783	-.00118966
35.46000000	1.01823729	3.25722582	-.02336842	-.14950585	.00107462
35.64000000	1.01461837	3.23411392	-.02010512	-.12817082	.00379953
35.82000000	1.01177372	3.21600463	-.01580359	-.10046594	.00731804
36.00000000	1.01019331	3.20596552	-.00878009	-.05572924	.01304281

MACH NO. = 2.500000 CD WAVE = .028562 SREF = 6.02628